iScience

CellPress
OPEN ACCESS

Article

GATA-4 overexpressing BMSC-derived exosomes suppress H/R-induced cardiomyocyte ferroptosis

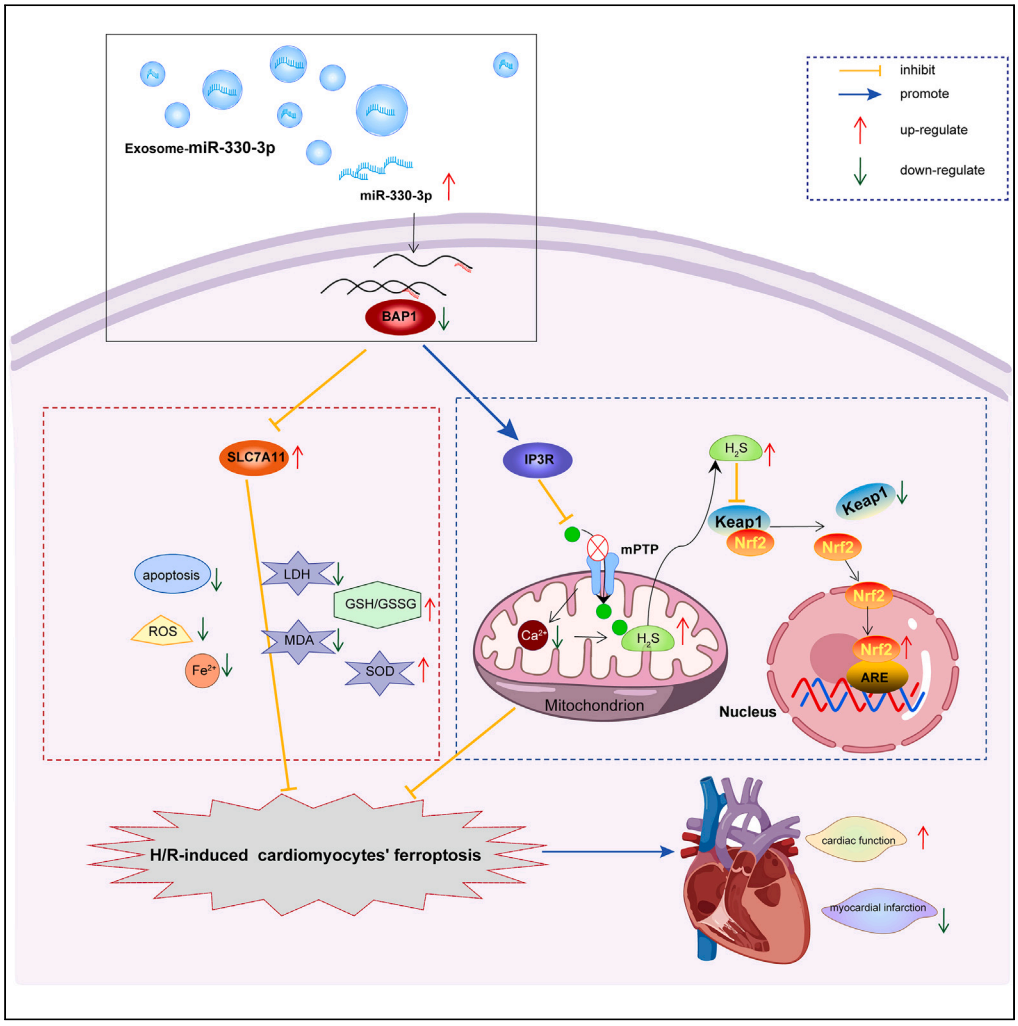

Zhiyuan Xiao, Si Li, Xinxin Wu, Xinhao Chen, Dan Yan, Jigang He

chouchou0708@aliyun.com

Highlights

Exos$^{oe-GATA-4}$ upregulates miR-330-3p in H/R-induced cardiomyocytes

miR-330-3p targeted negative regulated BAP1, BAP1 downregulates SLC7A11

BAP1 interacted with IP3R causing mPTP opening and mitochondrial dysfunction

Exos$^{oe-GATA-4}$ suppresses H/R-induced cardiomyocytes' ferroptosis and mPTP opening

Xiao et al., iScience 27, 110784
October 18, 2024
https://doi.org/10.1016/j.isci.2024.110784

iScience

CellPress
OPEN ACCESS

Article

GATA-4 overexpressing BMSC-derived exosomes suppress H/R-induced cardiomyocyte ferroptosis

Zhiyuan Xiao,[2,5] Si Li,[3,5] Xinxin Wu,[4] Xinhao Chen,[3] Dan Yan,[2] and Jigang He[1,6,*]

SUMMARY

Bone marrow mesenchymal stem cell (BMSC)-derived exosomes overexpressing GATA-4 ($Exos^{oe-GATA-4}$) can protect cardiac function. Mitochondrial permeability transition pore (mPTP) has a crucial role in ferroptosis. This study aimed to assess the mechanism of $Exos^{oe-GATA-4}$ in myocardial ischemia/reperfusion (I/R) injury. Exos were successfully excreted, and 185 differential expression miRNAs were obtained using bioinformatics. The $Exos^{oe-GATA-4}$ effectively suppressed hypoxia/reoxygenation (H/R)-induced cardiomyocytes' ferroptosis, while the effects were reversed by miR-330-3p inhibitor. miR-330-3p targeted negative regulated BAP1. The effects of miR-330-3p inhibitor were reversed by knock-down BAP1. Also, BAP1 reversed the effects of $Exos^{oe-GATA-4}$ on H/R-induced cardiomyocytes' ferroptosis by downregulating SLC7A11. Mechanistically, BAP1 interacted with IP3R and increased cardiomyocytes' Ca^{2+} level, causing mPTP opening and mitochondrial dysfunction, promoting H/R-induced cardiomyocytes' ferroptosis. Moreover, hydrogen sulfide (H_2S) content was increased and regulated the keap1/Nrf2 signaling pathway by $Exos^{oe-GATA-4}$ treated. $Exos^{oe-GATA-4}$ effectively suppresses H/R-induced cardiomyocytes' ferroptosis by upregulating miR-330-3p, which regulates the BAP1/SLC7A11/IP3R axis and inhibits mPTP opening.

INTRODUCTION

Cardiovascular diseases are the leading cause of death worldwide.[1] Acute myocardial infarction (AMI) is a serious condition caused by permanent damage to the heart muscle due to inadequate oxygen supply. At the moment, reperfusion remains the most effective treatment method for AMI[2]; timely reperfusion can salvage approximately 50% of severely ischemic myocardium.[3] However, cardiomyocyte injury and death that occur after ischemia/reperfusion (I/R) treatment, such as ferroptosis and pyroptosis, are irreversible.[4] Therefore, searching for effective treatment strategies to relieve cardiomyocyte injury after I/R is necessary for AMI patients.

Ferroptosis is a programmed cell death process characterized by a significant accumulation of lipid peroxides.[5] Studies have found that ferroptosis has a crucial role in myocardial I/R injury. For example, in diabetic patients with myocardial injury, ferroptosis is involved in the occurrence of myocardial injury.[6] In addition, Kajarabille et al. reported that ferroptosis inhibition can decrease the infarct size of transplanted I/R hearts and protect heart function.[7] Solute carrier family 7 member 11 (SLC7A11) is a crucial regulated protein of iron overload-ferroptosis,[8] which can increase cystine uptake and reduce the lipid peroxidation and ferroptosis that occur inside the cell.[9] Moreover, Zhang et al. found that BRCA1-associated protein 1 (BAP1), an anti-cancer gene, can regulate the ferroptosis-related gene SLC7A11 mediated ferroptosis.[10] Therefore, targeting SLC7A11 is a potential therapeutic strategy to prevent ferroptosis during myocardial I/R injury.

Mesenchymal stromal cells (MSCs) protect cardiac function by regulating cardioprotection, angiogenesis, and immunoregulation.[11] Moreover, studies have found that MSC-derived exosomes (MSC-Exos), rich in abundantly biologically active microRNAs, are essential for the capability of angiogenesis in treating myocardial infarction (MI).[12] In myocardial I/R injury, MSC-Exos can regulate the change between macrophages to M2 phenotype by miR-182 to relieve myocardial I/R injury.[13] In addition, Gao et al. found that several microRNAs highly expressed in MSC-Exos, especially miR-125a-5p, can be an effective therapy in I/R cardiac repair.[14]

Mitochondrial stress and dysfunction participate in ferroptosis by regulating Fe^{2+} and reactive oxygen species (ROS).[15] The opening of the mitochondrial permeability transition pore (mPTP), induced by Fe^{2+} and Ca^{2+},[16] which by inhibiting is a crucial factor in protecting the heart from the death of myocardial cells during I/R.[17] Previous research has confirmed that mPTP is the leading cause of cell death after reperfusion injury.[18] Overload of Ca^{2+} leads to mPTP opening, further inducing superoxide production, increased ROS, and cell ferroptosis.[19,20] Also,

[1]Department of Cardiovascular Surgery, the First People's Hospital of Yunnan Province, No.157 Jinbi Road, Kunming, Yunnan 650032, China
[2]Department of Medical Intensive Care Unit, the First People's Hospital of Yunnan Province, No.157 Jinbi Road, Kunming, Yunnan 650032, China
[3]The Affiliated Hospital of Kunming University of Science and Technology, Kunming 650500, P.R. China
[4]Yunnan University of Traditional Chinese Medicine, No.1076 Yuhua Road, Kunming, Yunnan 650500, China
[5]These authors contributed equally
[6]Lead contact
*Correspondence: chouchou0708@aliyun.com
https://doi.org/10.1016/j.isci.2024.110784

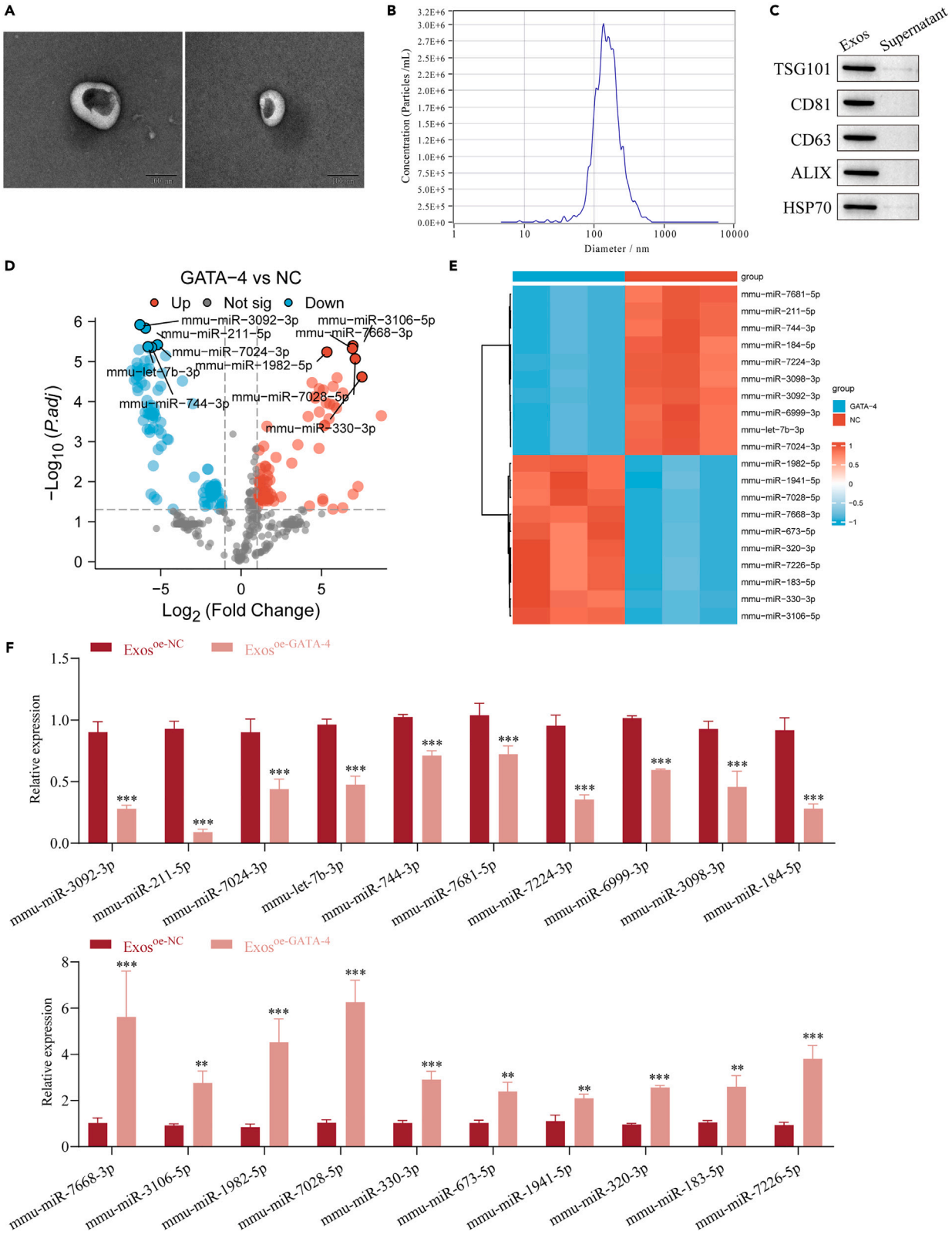
A
B
C
Concentration (Particles /mL)
Diameter / nm
Exos
Supernatant
TSG101
CD81
CD63
ALIX
HSP70
D
GATA−4 vs NC
Up
Not sig
Down
mmu−miR−3092−3p
mmu−miR−3106−5p
mmu−miR−211−5p
mmu−miR−7668−3p
mmu−miR−7024−3p
mmu−miR−1982−5p
mmu−let−7b−3p
mmu−miR−744−3p
mmu−miR−7028−5p
mmu−miR−330−3p
−Log10 (P.adj)
Log2 (Fold Change)
E
group
GATA−4
NC
mmu−miR−7681−5p
mmu−miR−211−5p
mmu−miR−744−3p
mmu−miR−184−5p
mmu−miR−7224−3p
mmu−miR−3098−3p
mmu−miR−3092−3p
mmu−miR−6999−3p
mmu−let−7b−3p
mmu−miR−7024−3p
mmu−miR−1982−5p
mmu−miR−1941−5p
mmu−miR−7028−5p
mmu−miR−7668−3p
mmu−miR−673−5p
mmu−miR−320−3p
mmu−miR−7226−5p
mmu−miR−183−5p
mmu−miR−330−3p
mmu−miR−3106−5p
F
Exos oe-NC
Exos oe-GATA-4
Relative expression
mmu-miR-3092-3p
mmu-miR-211-5p
mmu-miR-7024-3p
mmu-let-7b-3p
mmu-miR-744-3p
mmu-miR-7681-5p
mmu-miR-7224-3p
mmu-miR-6999-3p
mmu-miR-3098-3p
mmu-miR-184-5p
mmu-miR-7668-3p
mmu-miR-3106-5p
mmu-miR-1982-5p
mmu-miR-7028-5p
mmu-miR-330-3p
mmu-miR-673-5p
mmu-miR-1941-5p
mmu-miR-320-3p
mmu-miR-183-5p
mmu-miR-7226-5p

Figure 1. Differential expression miRNAs in BMSC-derived exosomes (Exos) overexpressing GATA-4 compared to BMSC-derived Exos^{oe-NC} group

(A) TEM image of Exos.

(B) NanoSight analysis.

(C) Western blot was used to evaluate exosome markers.

(D and E) Volcano plot (D) and heatmap (E) of differential expression miRNAs.

(F) RT-qPCR detected the expression levels of differential expression miRNAs. $n = 3$, $^{**}p < 0.01$, $^{***}p < 0.001$. Data are represented as mean ± SD.

inositol 1,4,5-triphosphate receptor (IP3R) has been reported as a regulated factor of Ca^{2+} levels that can induce Ca^{2+} release and raise the levels of Ca^{2+} in the cytosolic, further improving mitochondrial intake.[21,22] However, the mechanism of action of IP3R and mPTP has not been elucidated yet in myocardial I/R injury.

This study investigated the functional relationship between mPTP and myocardial I/R injury ferroptosis. Our results found that overexpression-GATA-4 BMSC-derived Exos effectively regulates the ferroptosis and is related to mPTP opening by BAP1/SLC7A11/IP3R axis via miR-330-3p, which also has an important role in cancer cell proliferation, apoptosis and migration, such as laryngeal squamous cell carcinoma,[23] gastric cancer,[24] and ovarian cancer.[25] Our findings elucidate an effective molecular mechanism of overexpression-GATA-4 BMSC-derived Exos in ferroptosis and identify the treatment strategy in myocardial I/R injury.

RESULTS

Differential expression miRNAs of overexpression-GATA-4 BMSC-derived exosome

Our previous study has confirmed that BMSC-derived exosomes (Exos) overexpressing GATA-4 can reduce anoxia-induced cardiomyocyte apoptosis and relieve myocardial infarction, in turn protecting cardiac function.[26] To further explore the exact mechanism involved in myocardial I/R injury, we extracted and identified the Exos. Exos showed a shape similar to a cup holder and a bilayer membrane (Figure 1A) with a particle size of 138.0 nm (Figure 1B; Data S1). Moreover, western blot was used to identify exosome markers, and it also had been verified that extracted Exos successfully (Figure 1C), TSG101, CD81, CD63, ALIX, and HSP70 only expressed in Exos.

Next, bioinformatics analysis was applied, and 185 differential expression miRNAs, including 104 downregulation and 81 upregulation, were detected (Table S1). The volcano plot is shown in Figure 1D, and the heatmap of each top 10 downregulation and upregulation differential expression miRNAs is shown in Figure 1E. Subsequently, we detected the expression of differential expression miRNAs; compared with Exos^{oe-NC} group, the expressions of mmu-miR-3092-3p, mmu-miR-211-5p, mmu-miR-7024-3p, mmu-let-7b-3p, mmu-miR-744-3p, mmu-miR-7681-5p, mmu-miR-7224-3p, mmu-miR-6999-3p, mmu-miR-3098-3p, and mmu-miR-184-5p were downregulated; the expressions of mmu-miR-7668-3p, mmu-miR-3106-5p, mmu-miR-1982-5p, mmu-miR-7028-5p, mmu-miR-330-3p, mmu-miR-673-5p, mmu-miR-1941-5p, mmu-miR-320-3p, mmu-miR-183-5p, and mmu-miR-7226-5p were upregulated in Exos overexpressing GATA-4 (Figure 1F).

BMSC-derived Exos overexpressing GATA-4 inhibits H/R-induced ferroptosis by upregulating miR-330-3p target-regulating BAP1

Based on preliminary research and studies, we identified miR-330-3p as a factor that may play an important role in cardiomyocyte I/R injury among many differential miRNAs, while the mechanism is unclear. Previous research has found that miR-330-3p plays a vital role in various cancers,[27,28] while the function in myocardial I/R injury has not been clearly stated. miR-330-3p is one of the differentially expressed miRNAs that effectively mediate AMI pathogenesis.[29] Moreover, miR-330-3p has been confirmed to suppress hepatic ischemia/reperfusion by regulating mitophagy.[30] Therefore, miR-330-3p may be an important regulatory factor as a differentially expressed miRNA. The aforementioned results have confirmed that miR-330-3p had a high expression in BMSC-derived Exos overexpressing GATA-4. To understand the mechanism of action of the Exos in myocardial I/R injury, we established cardiomyocytes I/R injury model *in vitro* by hypoxia/reoxygenation (H/R) induction.[31] To verify the success of the model construction, we performed reoxygenation for 2, 4, 6, and 8 h, and found increased malondialdehyde (MDA), ROS (Figures S1A and S1C) and apoptosis (Figure S1B), decreased superoxide dismutase (SOD) (Figure S1A) levels gradually as the reoxygenation time increased, had the best in 6 h. Subsequently, we evaluated the expression levels of hypoxia-inducible factor-1α (HIF-1α), B cell lymphoma-2 (Bcl-2), and Bcl-2-associated X (Bax) using RT-qPCR (Figure S1D) and western blot (Figure S1E), which showed that rose expression levels of HIF-1α and Bax, while lower expression levels of Bcl-2 as the reoxygenation time increases, also had the best with 6 h. Therefore, we chose hypoxia for 18 h and reoxygenation for 6 h to construct an H/R model that was a success, and then transfected cardiomyocytes with an NC inhibitor or miR-330-3p inhibitor (Figure 2A). The expression of miR-330-3p (Figure 2B) and cell viability (Figure 2C) increased in cardiomyocytes with BMSC-Exos $^{oe-NC}$, while cell apoptosis decreased (Figure 2D); yet, this effect was more pronounced in cardiomyocytes with BMSC-Exos overexpressing GATA-4 (Exos$^{oe-GATA-4}$). After adding miR-330-3p inhibitor, the expression of miR-330-3p and cell viability decreased, while cell apoptosis increased.

Subsequently, we assessed the content of lactate dehydrogenase (LDH), MDA, glutathione (GSH)/ oxidized glutathione (GSSG), and SOD, and levels of ROS and Fe^{2+}. The results showed that BMSC-Exos $^{oe-NC}$ had a particular effect on LDH, MDA, GSH/GSSG, SOD, ROS, and Fe^{2+} levels but it was not significant, while Exos$^{oe-GATA-4}$ significantly reduced the content of LDH, and MDA increased the GSH/GSSG ratio and content of SOD (Figure 2E), and reduced the levels of ROS (Figure 2F) and Fe^{2+} (Figure 2G). On the contrary, transfection with miR-330-3p

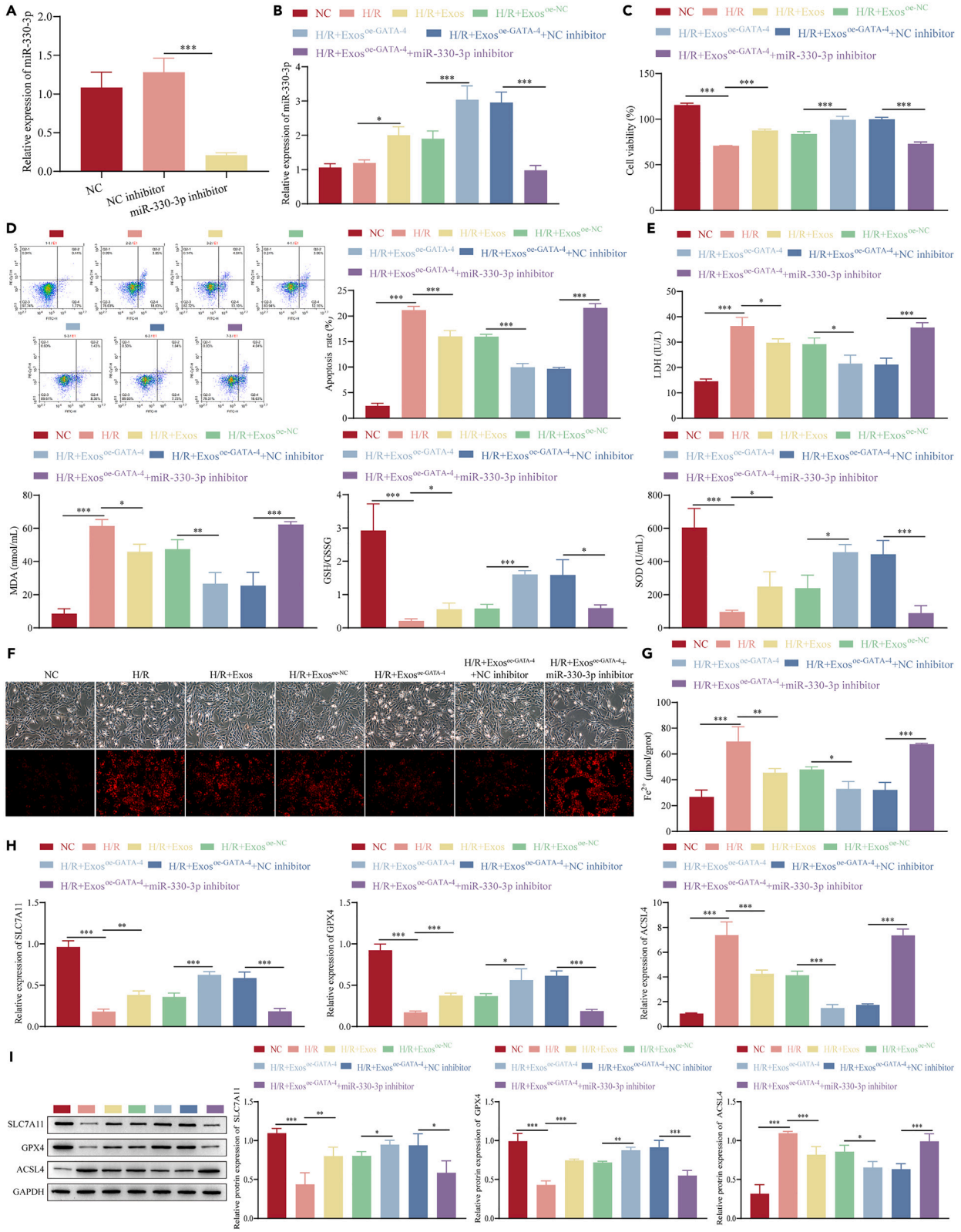
A
Relative expression of miR-330-3p
NC
NC inhibitor
miR-330-3p inhibitor
B
Relative expression of miR-330-3p
C
Cell viability (%)
D
Apoptosis rate (%)
E
LDH (IU/L)
MDA (nmol/mL)
GSH/GSSG
SOD (U/mL)
F
NC
H/R
H/R+Exos
H/R+Exos^oe-NC
H/R+Exos^oe-GATA-4
H/R+Exos^oe-GATA-4+NC inhibitor
H/R+Exos^oe-GATA-4+miR-330-3p inhibitor
G
Fe2+ (μmol/gprot)
H
Relative expression of SLC7A11
Relative expression of GPX4
Relative expression of ACSL4
I
SLC7A11
GPX4
ACSL4
GAPDH
Relative protrin expression of SLC7A11
Relative protrin expression of GPX4
Relative protrin expression of ACSL4

Figure 2. BMSC-derived exosomes overexpressing GATA-4 inhibits H/R-induced ferroptosis by upregulating miR-330-3p

(A and B) Transfection efficiency (A) and the expression of miR-330-3p (B) detected by RT-qPCR.

(C) CCK-8 assay.

(D) Flow cytometry assessing early and late cell apoptosis.

(E) The content of LDH, MDA, and GSH was detected by ELISA.

(F and G) The ROS (F) and Fe^{2+} (G) levels were detected by Kits assay.

(H and I) The expression levels of SLC7A11, GPX4, and ACSL4 were detected by RT-qPCR (H) and western blot (I). $n = 3$, $^{*}p < 0.05$, $^{**}p < 0.01$, $^{***}p < 0.001$. Data are represented as mean ± SD.

inhibitor reversed these effects; it increased the content of LDH and MDA, decreased the GSH/GSSG ratio and content of SOD and increased ROS and Fe^{2+} levels. The content of GSH and GSSG individually are shown in Figure S2.

In addition, $Exos^{oe-GATA-4}$ regulated the key proteins involved in ferroptosis, increased the expression levels of SLC7A11 and GPX4, and decreased the ACSL4 (Figures 2H and 2I); these effects were reversed by miR-330-3p inhibitor. The aforementioned results indicated that $Exos^{oe-GATA-4}$ can suppress H/R-induced cardiomyocytes' ferroptosis by upregulating miR-330-3p.

To clarify the mechanism further, we predicted the target genes of miR-330-3p, a total of 3,965 genes (Table S2). Cytoscape software visualized the target relation of genes (Figure 3A; Table S3). Interestingly, among them, BAP1's high expression is related to ferroptosis, which is a driver gene in ferroptosis, which can inhibit cystine uptake, decrease GSH levels, and increase ROS accumulation.[10,32] Hence, we further verified the relationship between miR-330-3p and BAP1, and found that BAP1 was the target gene of miR-330-3p; the combined sequence shown in Figure 3B indicated that BAP1 contains targeted binding sites for miR-330-3p. The results of the dual-luciferase reporter assay showed that miR-330-3p mimic reduced the luciferase activity of BAP1-WT, while it did not affect BAP1-MUT (Figure 3C). AgO2-RIP assay further confirmed this relationship; miR-330-3p mimic increased the expression of BAP1 in the AgO2 group (Figure 3D). In summary, the results showed targeted binding between miR-330-3p and BAP1.

We then co-transfected si-NC and si-BAP1 into cardiomyocytes and examined the transfection efficiency by RT-qPCR (Figure 3E) and western blot (Figure 3F). $Exos^{oe-GATA-4}$ reduced the expression of BAP1, while miR-330-3p inhibitor reversed this process. When cells were co-transfected with si-BAP1, the expression level was further decreased (Figures 3G and 3H).

We further explored the effect of BAP1 in H/R-induced cardiomyocyte ferroptosis and found that the cell viability was decreased in cardiomyocytes with the $Exos^{oe-GATA-4}$+miR-330-3p inhibitor. Yet, co-transfection of cardiomyocytes with si-BAP1 further increased the cell viability (Figure 4A). The miR-330-3p inhibitor promoted cell apoptosis; in contrast, this process was reversed after co-transfected with si-BAP1 (Figure 4B). Also, the $Exos^{oe-GATA-4}$+miR-330-3p inhibitor group significantly increased the content of LDH and MDA, decreased the GSH/GSSG ratio and content of SOD, and raised the levels of ROS and Fe^{2+}; while co-transfection with si-BAP1 reversed these effects (Figures 4C–4E). The content of GSH and GSSG individually are shown in Figure S3. In addition, the $Exos^{oe-GATA-4}$+miR-330-3p inhibitor group decreased the expression levels of SLC7A11 and GPX4 and increased the ACSL4, which was analyzed by RT-qPCR and western blot (Figures 4F and 4G); these effects were reversed by co-transfected si-BAP1. These results confirmed that $Exos^{oe-GATA-4}$ effectively suppressed H/R-induced cardiomyocytes' ferroptosis by miR-330-3p targeted negative regulated the expression of BAP1.

BAP1 reverses the inhibiting role of overexpression-GATA-4 BMSC-derived exosome H/R-induced cardiomyocytes ferroptosis by downregulating target gene SLC7A11

Interestingly, solute carrier family 7 member 11 (SLC7A11) is a crucial regulated protein of ferroptosis, which has been reported as the target gene of BAP1.[10,33] Therefore, we further verified the mechanism of BAP1 and SLC7A11 in H/R-induced cardiomyocyte ferroptosis. Luciferase reporter assay showed that BAP1-WT could reduce the SLC7A11 promoter, while BAP1-MUT had no effect on the promoter. Also, knock down of BAP1 could increase the SLC7A11 promoter (Figure 5A).

We then transfected oe-NC and oe-BAP1 into cardiomyocytes and examined the transfection efficiency by RT-qPCR (Figure 5B) and western blot (Figure 5C). Western blot data showed that overexpression of BAP1 could reduce the expression of SLC7A11, while the knock down of BAP1 increased the expression (Figure 5D).

Then, we co-transfected oe-NC and oe-SLC7A11 into cardiomyocytes and examined the transfection efficiency by RT-qPCR (Figure 5E) and western blot (Figure 5F). $Exos^{oe-GATA-4}$ increased the expression of SLC7A11, while after transfection with oe-BAP1, expression levels decreased; when co-transfected with oe-SLC7A11, the expression level further increased (Figures 5G and 5H). These results show that BAP1 negatively regulates the expression of SLC7A11.

The CCK-8 assay showed that the effect of $Exos^{oe-GATA-4}$ on cell viability was reversed by overexpression of BAP1, while overexpression of SLC7A11 increased cell viability (Figure 6A). Also, overexpression of BAP1 promoted cell apoptosis, which was reversed by overexpression SLC7A11 (Figure 6B). Subsequently, the results showed that the $Exos^{oe-GATA-4}$+oe-BAP1 group significantly increased the content of LDH and MDA, decreased the GSH/GSSG ratio and content of SOD, and raised the levels of ROS and Fe^{2+}. On the contrary, co-transfection with oe-SLC7A11 reversed this process (Figures 6C–6E). The content of GSH and GSSG individually are shown in Figure S4. In addition, overexpression of BAP1 reversed the effects of $Exos^{oe-GATA-4}$, decreased the expression levels of SLC7A11 and GPX4, and increased the ACSL4, which was analyzed by RT-qPCR and western blot (Figures 6F and 6G). Similarly, overexpression of SLC7A11 further reversed the effects. These results confirmed that BAP1 reverses the effects of $Exos^{oe-GATA-4}$ suppressed H/R-induced cardiomyocytes' ferroptosis by downregulating the expression of SLC7A11.

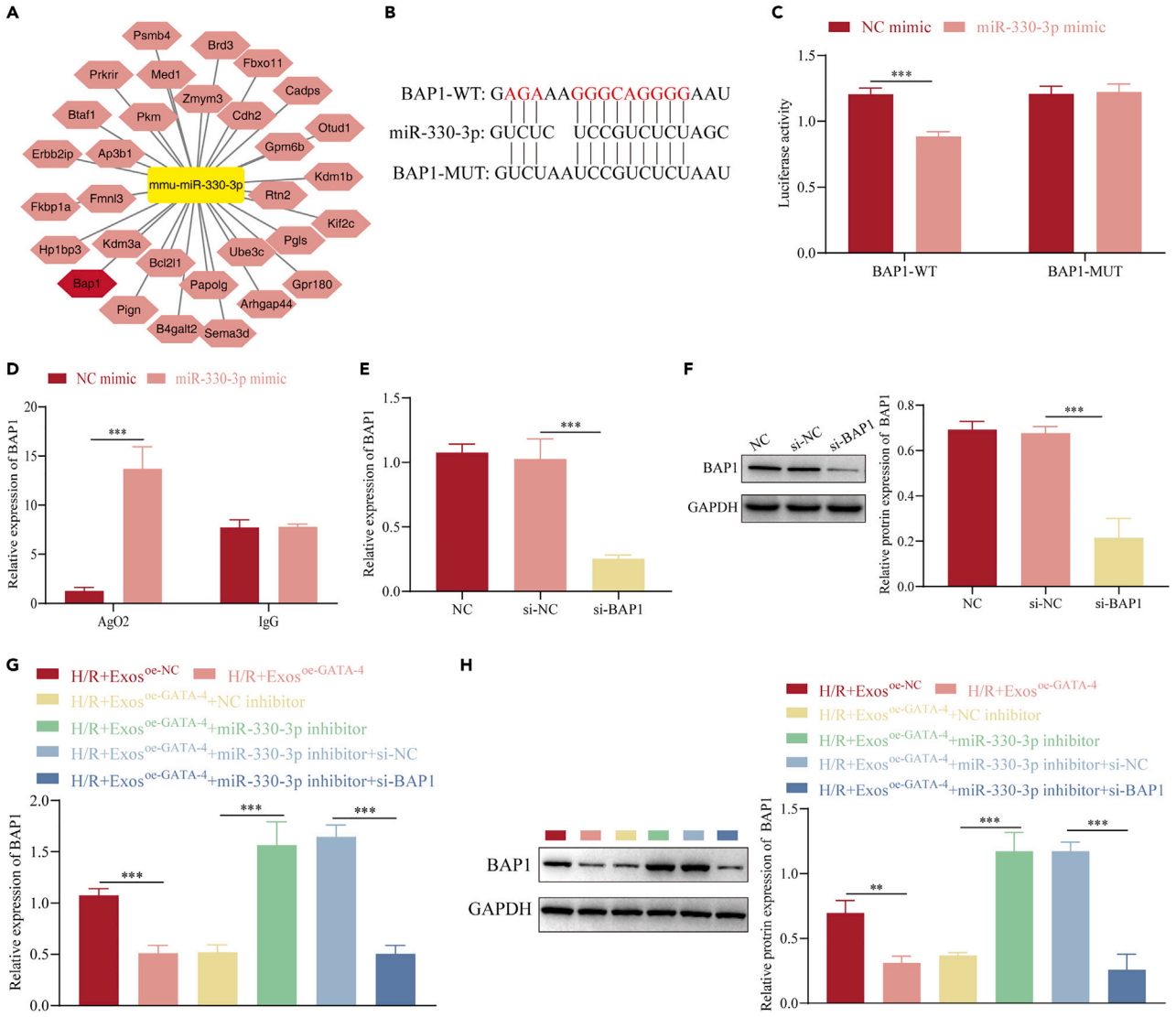

Figure 3. miR-330-3p target-regulating BAP1

(A) Cytoscape software visualization (only shows the 31 target genes).

(B) The combined sequence between miR-330-3p and BAP1.

(C) Dual-luciferase reporter assay.

(D) AgO2-RIP assay.

(E and F) Transfection efficiency of si-NC and si-BAP1 in cardiomyocytes was detected by (E) RT-qPCR and western blot (F).

(G and H) The expression levels of BAP1 were detected by RT-qPCR (G) and western blot (H). $n = 3$, $^{**}p < 0.01$, $^{***}p < 0.001$. Data are represented as mean ± SD.

BAP1 induces cardiomyocytes Ca^{2+} overload, leading to mPTP activation and mitochondrial dysfunction by interacting with IP3R

The mitochondrial permeability transition pore (mPTP) has a crucial role in cardiomyocyte H/R injury; the increased Ca^{2+} induces mPTP opening and causes cardiomyocyte apoptosis.[34,35] Inositol 1,4,5-triphosphate receptor (IP3R) has been confirmed to regulate cytosolic Ca^{2+} levels and promote the activation of mitochondrial calcium uniporter (MCU), involved in mPTP opening.[21,36] In our study, co-immunoprecipitation (coIP) and glutathione S-transferase (GST) pull-down assays showed that in cardiomyocytes, BAP1 protein interacts with IP3R protein (Figure 7A), and GST-labeled BAP1 protein could pull down GST-labeled IP3R protein (Figure 7B). These results further confirmed a close interaction between BAP1 and IP3R. Overexpression of BAP1 significantly increased the expression of IP3R, while the knock down of BAP1 reduced the expression (Figures 7C and 7D).

We then transfected si-NC and si-IP3R into cardiomyocytes and examined the transfection efficiency by RT-qPCR (Figure 7E) and western blot (Figure 7F), the expression of IP3R was decreased after knock down of IP3R, which indicated that transfection was successful. The

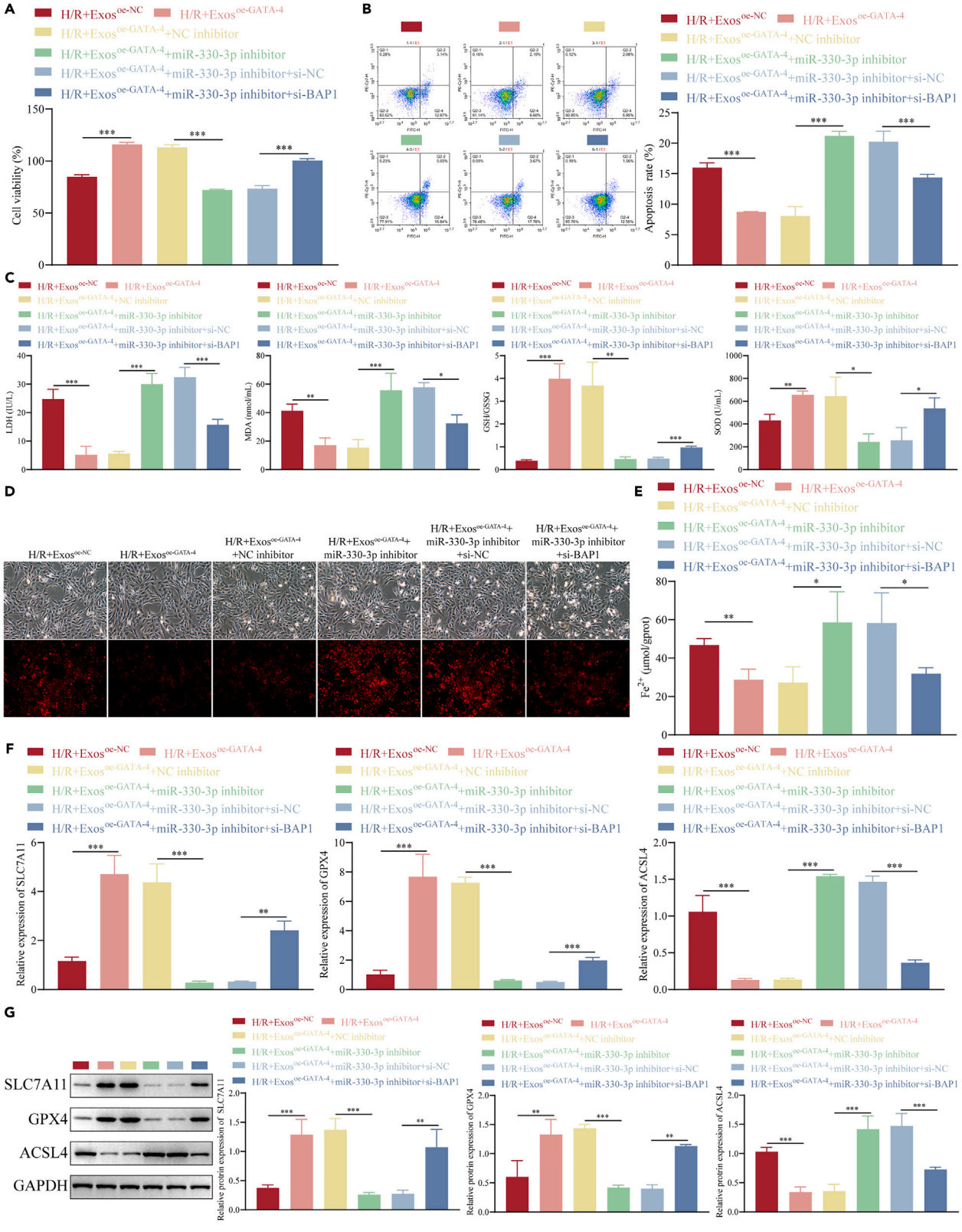
A
B
C
D
E
F
G
H/R+Exos^oe-NC
H/R+Exos^oe-GATA-4
H/R+Exos^oe-GATA-4+NC inhibitor
H/R+Exos^oe-GATA-4+miR-330-3p inhibitor
H/R+Exos^oe-GATA-4+miR-330-3p inhibitor+si-NC
H/R+Exos^oe-GATA-4+miR-330-3p inhibitor+si-BAP1
Cell viability (%)
Apoptosis rate (%)
LDH (IU/L)
MDA (nmol/mL)
GSH/GSSG
SOD (U/mL)
Fe2+ (μmol/gprot)
Relative expression of SLC7A11
Relative expression of GPX4
Relative expression of ACSL4
SLC7A11
GPX4
ACSL4
GAPDH
Relative protein expression of SLC7A11
Relative protein expression of GPX4
Relative protein expression of ACSL4

Figure 4. BMSC-derived exosomes overexpressing GATA-4 inhibits H/R-induced cardiomyocyte ferroptosis by miR-330-3p target-regulating BAP1

(A) CCK-8 assay.

(B) Early and late cell apoptosis detected by flow cytometry.

(C) The content of LDH, MDA, and GSH was detected by ELISA.

(D and E) The ROS (D) and Fe^{2+} (E) levels were detected by Kits assay.

(F and G) The expression levels of SLC7A11, GPX4 and ACSL4 were detected by RT-qPCR (F) and western blot (G). $n = 3$, $^{*}p < 0.05$, $^{**}p < 0.01$, $^{***}p < 0.001$. Data are represented as mean ± SD.

expression of IP3R was reduced in the $Exos^{oe-GATA-4}$ group, while transfected oe-BAP1 increased these levels significantly. In addition, after being co-transfected with si-IP3R, the expression level of IP3R further decreased (Figures 7G and 7H).

To further explore the function of BAP1 and IP3R in mPTP opening, we analyzed the Ca^{2+} levels in cardiomyocytes. $Exos^{oe-GATA-4}$ significantly decreased the level of Ca^{2+}, while BAP1 overexpression reversed this process. In contrast, after co-transfected si-IP3R, the level was further reduced (Figure 7I). The mPTP opening analysis showed that $Exos^{oe-GATA-4}$ significantly inhibited the mPTP opening, while the overexpression of BAP1 promoted mPTP opening. At the same time, knock down of IP3R relieved the function and inhibited mPTP opening (Figure 8A). Also, the MCU mRNA and protein expression levels were decreased in the $Exos^{oe-GATA-4}$ group. After transfection with oe-BAP1, the levels further increased, while the knock down of IP3R reversed the effect of oe-BAP1 (Figures 8B and 8C). Similarly, JC-1 monomers and CyP-D fluorescence expression were decreased in the $Exos^{oe-GATA-4}$ group; in the $Exos^{oe-GATA-4}$ +oe-BAP1 group, the fluorescence expression was further increased, while after cells were co-transfected si-IP3R, the effects were inhibited (Figures 8D and 8E). Consistently, mitochondrion swelling and disruption of the bilayer membrane were seen in the $Exos^{oe-GATA-4}$ +oe-BAP1 group but relieved in the $Exos^{oe-GATA-4}$ +oe-BAP1+si-IP3R group (Figure 8F). These results indicated that BAP1 increases cardiomyocytes' Ca^{2+} level, inducing mPTP opening and mitochondrial dysfunction through interactions with IP3R.

BAP1 induced mPTP opening reverses the inhibiting role of BMSC-derived $Exos^{oe-GATA-4}$ on H/R-induced cardiomyocytes ferroptosis by interacting with IP3R

To further explore the function mechanism of mPTP opening in H/R-induced cardiomyocyte ferroptosis, cardiomyocytes were treated with mPTP inhibitor (CsA). Overexpression of BAP1 significantly reduced cell viability (Figure 9A) and promoted cell apoptosis (Figure 9B), while CsA reversed these results. Also, the $Exos^{oe-GATA-4}$+oe-BAP1 group significantly increased the content of LDH and MDA, decreased the GSH/GSSG ratio and content of SOD, and increased the levels of ROS and Fe^{2+}; these effects were reversed by CsA (Figures 9C–9E). The content of GSH and GSSG individually are shown in Figure S5. Subsequently, the results of RT-qPCR and western blot also confirmed that CsA reversed the role of the $Exos^{oe-GATA-4}$+oe-BAP1 group, increased the expression levels of SLC7A11 and GPX4, and decreased the ACSL4 (Figures 9F and 9G). These results confirmed that overexpression-GATA-4 BMSC-derived exosome inhibits H/R-induced cardiomyocyte ferroptosis through BAP1 interacts with IP3R inhibited mPTP opening.

BMSC-derived $Exos^{oe-GATA-4}$ inhibits H/R-induced cardiomyocytes ferroptosis related with keap1/Nrf2 signaling pathway

Previous studies have shown that H_2S can regulate the mPTP opening in cardiomyocytes,[37] and Ca^{2+} induces mPTP opening blocked by high levels of H_2S.[38] Moreover, H_2S production can further reduce lipid peroxide levels and inhibit ferroptosis,[39] which may be related to the keap1/Nrf2 signaling pathway.[40] In our study, we further observed that the hydrogen sulfide (H_2S) content increased in the $Exos^{oe-GATA-4}$ group. Yet, after overexpressing BAP1, the H_2S content decreased. At the same time, CsA further increased the H_2S content (Figure 10A). In addition, the results of RT-qPCR and western blot showed that the expression levels of keap1 were decreased, and Nrf2 was increased in the $Exos^{oe-GATA-4}$ group, while after overexpressing BAP1, keap1 increased and Nrf2 decreased. Similarly, these results were reversed by CsA (Figures 10B and 10C).

We further used immunofluorescence (IF) to review the expression situation of Nrf2 and found that expressed in the cytoplasm, while the $Exos^{oe-GATA-4}$ group and $Exos^{oe-GATA-4}$+oe-BAP1+CsA group increased the expression in the nucleus (Figure 10D). Therefore, our results showed that $Exos^{oe-GATA-4}$ may have regulated the keap1/Nrf2 signaling pathway through released H_2S, inhibiting H/R-induced cardiomyocyte ferroptosis.

BMSC-derived $Exos^{oe-GATA-4}$ inhibits I/R-induced cardiomyocytes ferroptosis by upregulating miR-330-3p *in vivo*

I/R mice model treated with $Exos^{oe-NC}$, $Exos^{oe-GATA-4}$, NC inhibitor, and miR-330-3p inhibitor by tail vein injection was assessed next. Compared with the Sham group, ejection fraction (EF) and fractional shortening (FS) levels decreased, and impaired cardiac function (Figure 11A) and infarction area increased (Figure 11B) in the I/R and I/R+$Exos^{oe-NC}$ group, while these effects were relieved in the I/R+$Exos^{oe-GATA-4}$ group. In contrast, in the I/R+$Exos^{oe-GATA-4}$+miR-330-3p inhibitor group, heart damage and infarction were more obvious.

Subsequently, we detected the levels of Fe^{2+} and MDA. In the I/R and I/R + $Exos^{oe-NC}$ group, Fe^{2+} and MDA increased, while they decreased in the I/R+$Exos^{oe-GATA-4}$ group. Conversely, in the I/R+$Exos^{oe-GATA-4}$+miR-330-3p inhibitor group, the levels of Fe^{2+} and MDA further increased (Figures 11C and 11D). At the same time, the GSH/GSSG level was decreased by I/R-induced, which was increased in the I/R+$Exos^{oe-GATA-4}$ group; on the contrary, the I/R+$Exos^{oe-GATA-4}$+miR-330-3p inhibitor group further reduced that (Figure S6A). The results of RT-qPCR and western blot further showed that the expression levels of miR-330-3p, SLC7A11, and GPX4 were increased in the I/R+$Exos^{oe-GATA-4}$ group; while BAP1, IP3R, and ACSL4 were decreased; in the I/R+$Exos^{oe-GATA-4}$+miR-330-3p inhibitor group these data were

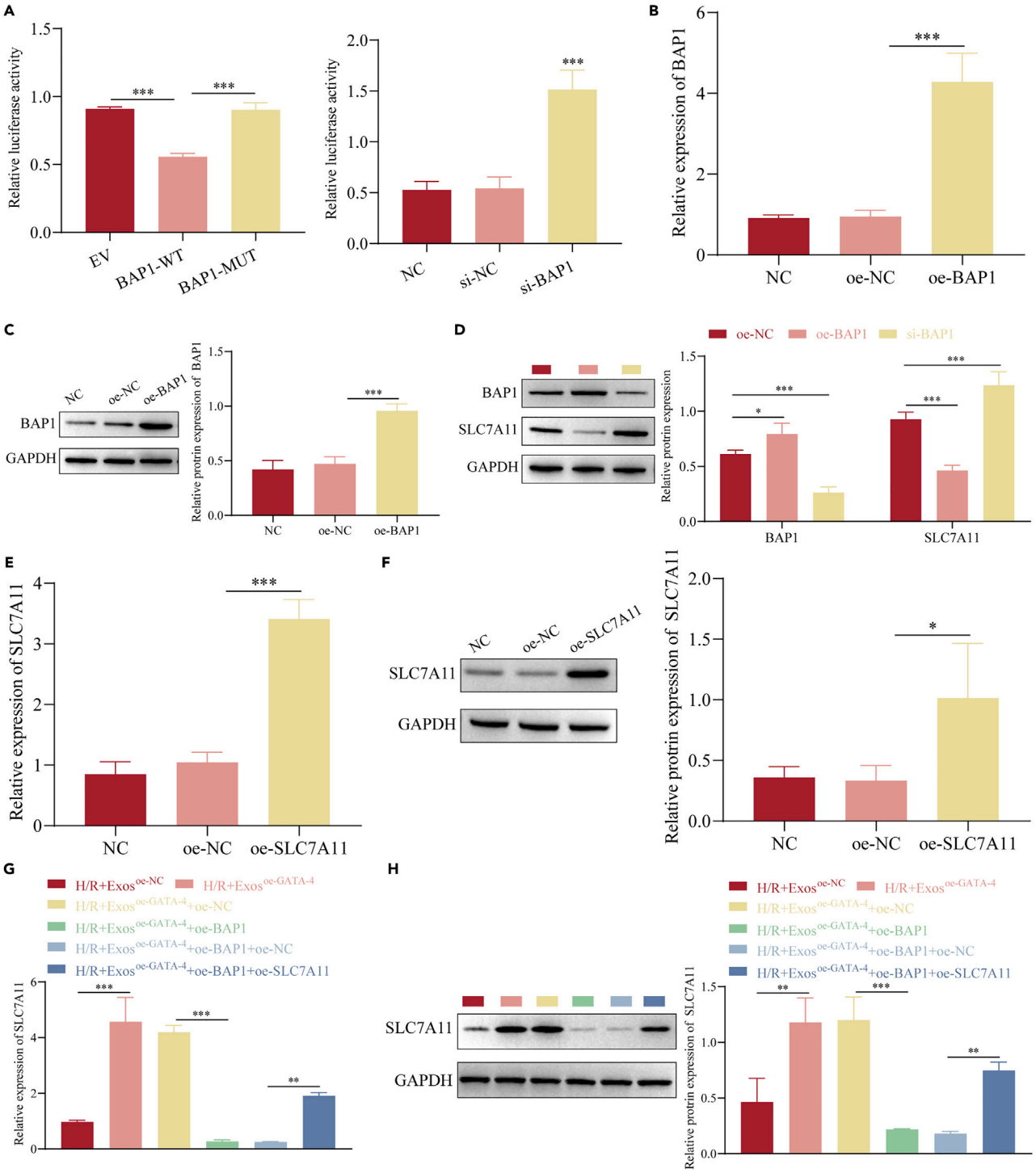

Figure 5. BAP1 negative regulated the expression of SLC7A11

(A) Luciferase reporter assay. AgO2-RIP assay.

(B and C) Transfection efficiency of oe-NC and oe-BAP1 in cardiomyocytes was detected by RT-qPCR (B) and western blot (C).

(D) The expression levels of BAP1 and SLC7A11 were detected by western blot.

(E and F) Transfection efficiency of oe-NC and oe-SLC7A11 in cardiomyocytes was detected by RT-qPCR (E) and western blot (F).

(G and H) The expression levels of SLC7A11 were detected by RT-qPCR (G) and western blot (H). $n = 3$, $^{*}p < 0.05$, $^{**}p < 0.01$, $^{***}p < 0.001$. Data are represented as mean ± SD.

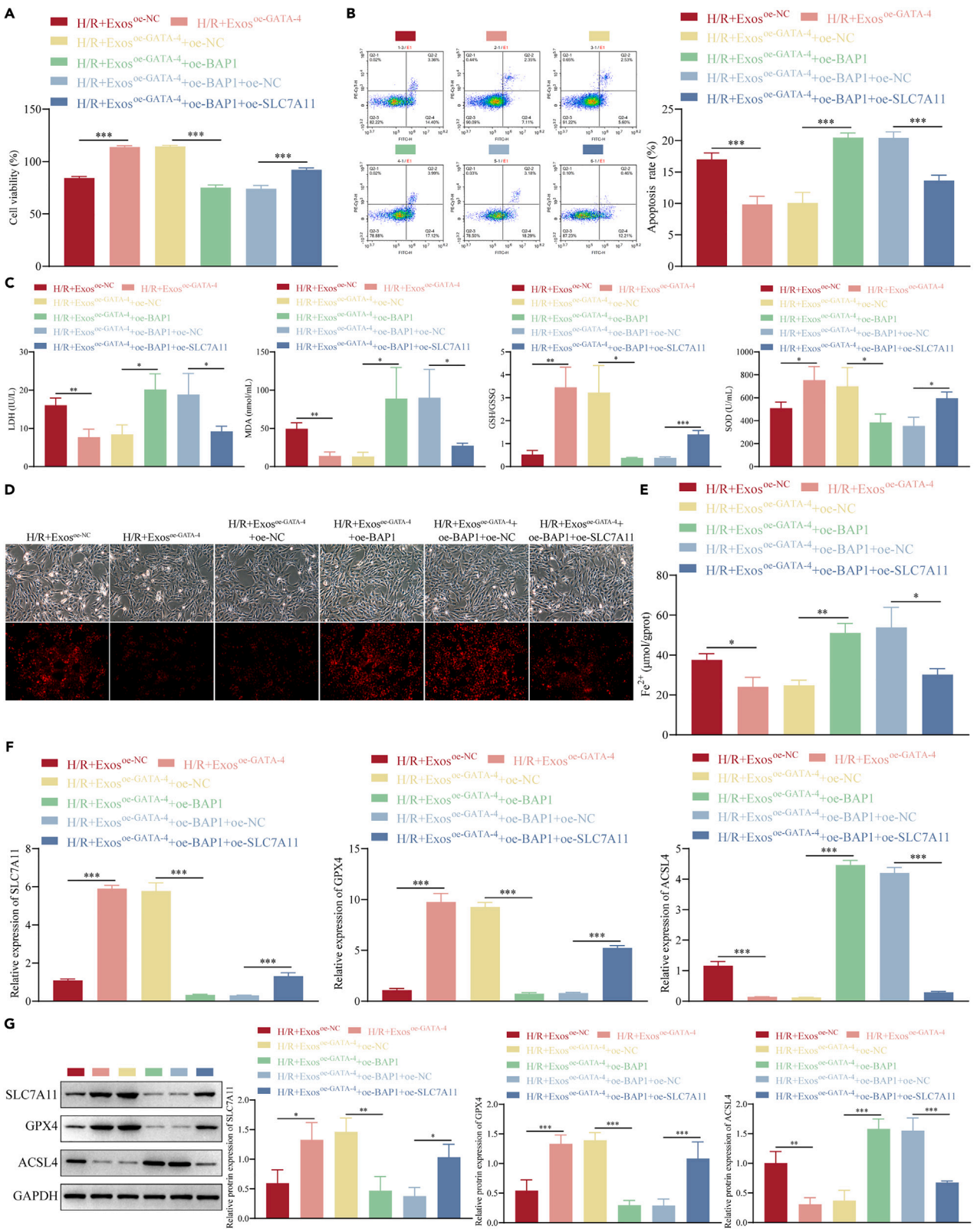
A
H/R+Exos^oe-NC
H/R+Exos^oe-GATA-4
H/R+Exos^oe-GATA-4+oe-NC
H/R+Exos^oe-GATA-4+oe-BAP1
H/R+Exos^oe-GATA-4+oe-BAP1+oe-NC
H/R+Exos^oe-GATA-4+oe-BAP1+oe-SLC7A11
Cell viability (%)
B
Apoptosis rate (%)
C
LDH (IU/L)
MDA (nmol/mL)
GSH/GSSG
SOD (U/mL)
D
H/R+Exos^oe-NC
H/R+Exos^oe-GATA-4
H/R+Exos^oe-GATA-4 +oe-NC
H/R+Exos^oe-GATA-4 +oe-BAP1
H/R+Exos^oe-GATA-4+ oe-BAP1+oe-NC
H/R+Exos^oe-GATA-4+ oe-BAP1+oe-SLC7A11
E
Fe2+ (μmol/gprot)
F
Relative expression of SLC7A11
Relative expression of GPX4
Relative expression of ACSL4
G
SLC7A11
GPX4
ACSL4
GAPDH
Relative protrin expression of SLC7A11
Relative protrin expression of GPX4
Relative protrin expression of ACSL4

Figure 6. BAP1 reverses the inhibiting role of BMSC-derived exosome overexpressing GATA-4 on H/R-induced cardiomyocyte ferroptosis by downregulating target gene SLC7A11

(A) CCK-8 assay.

(B) Early and late cell apoptosis detected by flow cytometry.

(C) The content of LDH, MDA, and GSH was detected by ELISA.

(D and E) The ROS (D) and Fe^{2+} (E) levels were detected by Kits assay.

(F and G) The expression levels of SLC7A11, GPX4, and ACSL4 were detected by RT-qPCR (F) and western blot (G). $n = 3$, $^{*}p < 0.05$, $^{**}p < 0.01$, $^{***}p < 0.001$. Data are represented as mean ± SD.

reversed (Figure 11E). Moreover, we further estimated the expression of Keap1/Nrf2; the results of RT-qPCR (Figure S6B) and western blot (Figure S6C) showed the expression of Keap1 was increased, and Nrf2 was reduced by I/R-induced. Keap1 was further decreased, and Nrf2 was further rose by $Exos^{oe-GATA-4}$. The I/R+Exosoe-GATA-4+miR-330-3p inhibitor group showed a reversal trend. These results suggest that BMSC-derived exosome overexpressing GATA-4 inhibits I/R-induced cardiomyocyte ferroptosis by increasing the expression levels of miR-330-3p.

DISCUSSION

Our previous research demonstrated that BMSC-derived exosome overexpressing GATA-4 ($Exos^{oe-GATA-4}$) can protect cardiac function and inhibit cardiomyocyte apoptosis.[26] However, the specific mechanism of action of $Exos^{oe-GATA-4}$ in myocardial I/R injury remains unclear. In this study, we successfully extracted and identified the Exos and obtained 185 differential expression miRNAs by bioinformatics analysis, including 104 downregulated and 81 upregulated miRNAs. Among the upregulated miRNAs, we assessed mmu-miR-330-3p further. miR-330-3p has a crucial role in I/R injury and apoptosis.[30] However, its function in myocardial I/R injury is still not fully understood. Herein, we found that $Exos^{oe-GATA-4}$ can inhibit I/R-induced cardiomyocyte ferroptosis by upregulating the expression of miR-330-3p and related to Ca^{2+} overload and mPTP opening.

miRNAs in Exos regulate function during intercellular communication.[41] BMSC-derived Exos has multiple functions; for example, they promote skeletal muscle regeneration,[42] participate in lung cancer metastasis,[43] and can ameliorate osteoarthritis.[44] They also have a crucial role in cardiomyocyte injury. Mao et al. confirmed that miR-183-5p found in BMSC-derived Exos inhibits cardiomyocyte apoptosis and protects myocardial I/R injury.[45] Previous studies have also shown that miR-330-3p is a differentially expressed miRNA in kynurenine-treated BMSC cultures.[46] This is consistent with our findings, which show that miR-330-3p is one of the upregulation differential expression miRNAs in $Exos^{oe-GATA-4}$. BMSC-derived exosomes are a valid treatment method for ischemic injury; BMSC-derived Exos miR-148b-3p further strengthen BMSC-derived Exos effects, which are used in treating cerebral ischemia.[47] Therefore, miRNA is a crucial regulatory factor for the BMSC-derived Exos role. Exos also exert a role in cancer by inhibiting miR-330-3p.[48] Previous research has found that miR-330-3p plays a vital role in various cancers,[27,28] while the function in myocardial I/R injury has not been clearly stated. miR-330-3p is one of the differentially expressed miRNAs that effectively mediate AMI pathogenesis.[29] However, the $Exos^{oe-GATA-4}$ and miR-330-3p functions in I/R-induced cardiomyocyte ferroptosis have not been reported. Interestingly, hypoxia-preconditioned brain cells (brain-EVs)-derived extracellular vesicles decreased infarct size in neonatal hypoxic-ischemic brain injury (HIBI) and consistently expressed miR-330-3p,[49] this seems to coincide with our results. This study discovered that $Exos^{oe-GATA-4}$ could effectively suppress H/R-induced cardiomyocytes' ferroptosis by upregulating miR-330-3p. Moreover, Exosoe-GATA-4 also increased the GSH/GSSH ratio and reduced ROS accumulation. ROS accumulation induces myocardial cell injury and is related to low GSH content, which can participate in clearance.[50,51] GSH plays a vital role in maintaining redox homeostasis in cardiomyocytes. Disruption of redox homeostasis is evidenced by a significant decrease in GSH content and accumulation of GSSG and ROS in the myocardium. GSH has been confirmed to relieve myocardial injury by inhibiting ferroptosis. Maintaining an optimal GSH/GSSG ratio in the myocardium is essential for maintaining homeostatic cell survival. Moreover, GSH and glutathione peroxidase 4 (GPX4) are intimately associated with ferroptosis.[52] ROS and GSH are the core participants in ferroptosis; GSH depletion and GPX4 inactivation have been confirmed to lead to ferroptosis.[53]

miR-330-3p plays multiple effects by regulating direct targets, such as in glioma cells, miR-330-3p inhibits cell proliferation and migration by regulating the target gene CELF1,[54] miR-330-3p promotes the non-small-cell lung cancer (NSCLC) malignant progression through targeting GRIA3.[55] Our study also found that BAP1 is the target gene of miR-330-3p. BAP1 functions as a tumor suppressor and is essential in cellular metabolism.[56] Also, BAP1 participates in ferroptosis,[57] which is a driver gene in ferroptosis, which can inhibit cystine uptake, decrease GSH levels, and increase ROS accumulation.[10,32] Our results further confirmed that the effects of $Exos^{oe-GATA-4}$ suppress H/R-induced cardiomyocytes' ferroptosis through miR-330-3p targeted negative regulated BAP1, at the same time, increase the GSH/GSSG ratio and reduce ROS accumulation. It is widely acknowledged that GPX4 and SLC7A11 are critical regulatory proteins involved in ferroptosis. Loss of GSH is a key mechanism in ferroptosis occurrence; SLC7A11 has been confirmed to be necessary for intracellular GSH production to inhibit ferroptosis.[58] SLC7A11 overexpression can relieve ferroptosis in various cancer cells[59,60] and myocardial cells.[61] Furthermore, we further demonstrated that BAP1 is capable of reducing the expression of SLC7A11. BAP1 reverses the suppressing effects of $Exos^{oe-GATA-4}$ on H/R-induced cardiomyocytes' ferroptosis by downregulating the expression of SLC7A11, decreasing the GSH/GSSH ratio. BAP1 has been demonstrated to regulate SLC7A11 expression and ferroptosis in previous research, BAP1 regulates the expression of SLC7A11 independently of other transcription factors. BAP1 reduces the presence of H2A ubiquitination (H2Aub) on the SLC7A11 promoter and suppresses the expression of SLC7A11 in a deubiquitinating-dependent manner. Additionally, BAP1 hinders cystine uptake by repressing SLC7A11 expression, which leads to

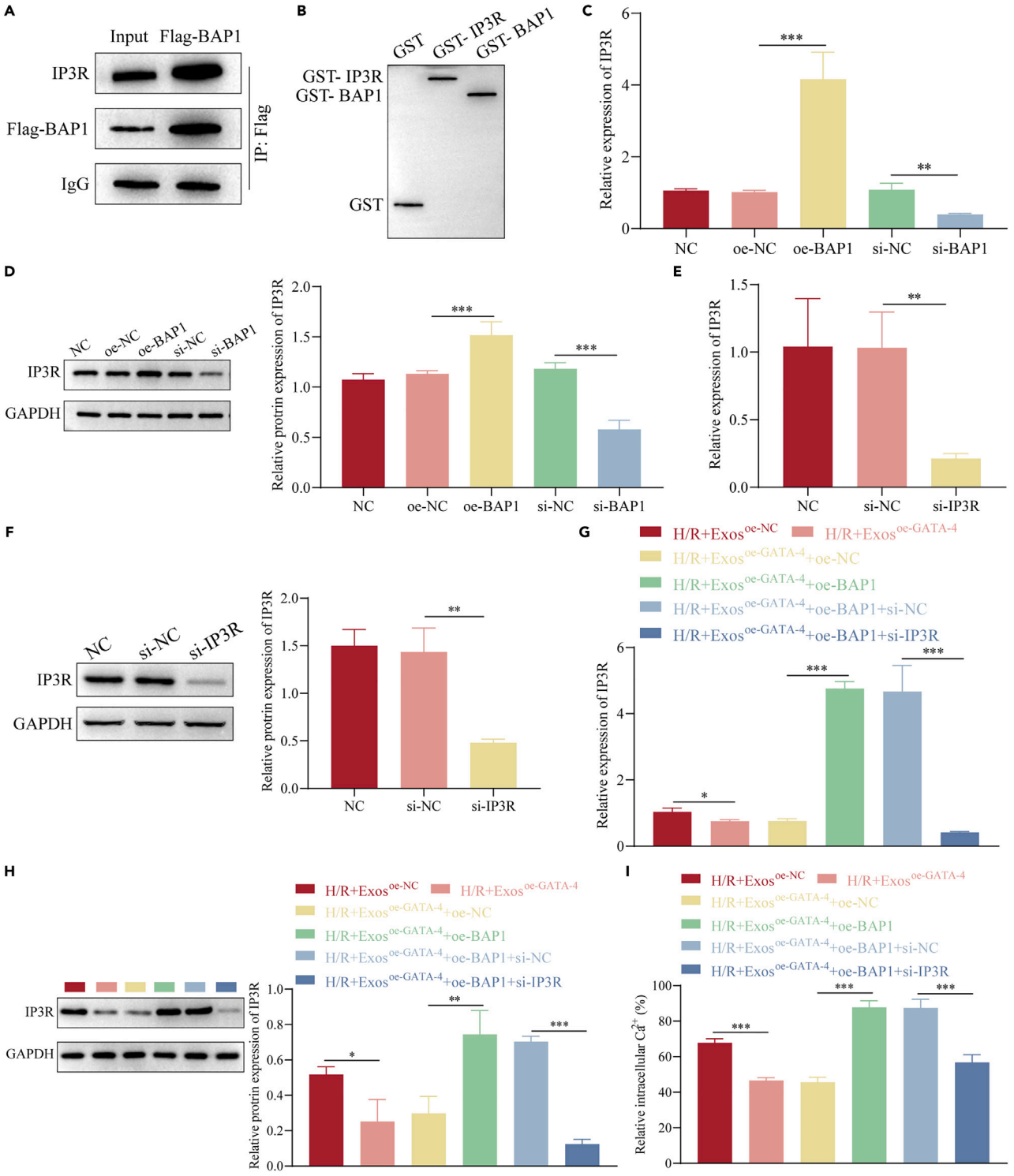

Figure 7. BAP1 interacts with IP3R

(A) CoIP assay.

(B) GST pull-down assay.

(C and D) The expression levels of IP3R were detected by (C) RT-qPCR and western blot (D).

(E and F) Transfection efficiency of si-NC and si-IP3R in cardiomyocytes was detected by RT-qPCR (E) and western blot (F).

(G and H) The expression levels of IP3R were detected by RT-qPCR (G) and western blot (H).

(I) The Ca^{2+} levels were detected by Kits assay. $n = 3$, $^{*}p < 0.05$, $^{**}p < 0.01$, $^{***}p < 0.001$. Data are represented as mean ± SD.

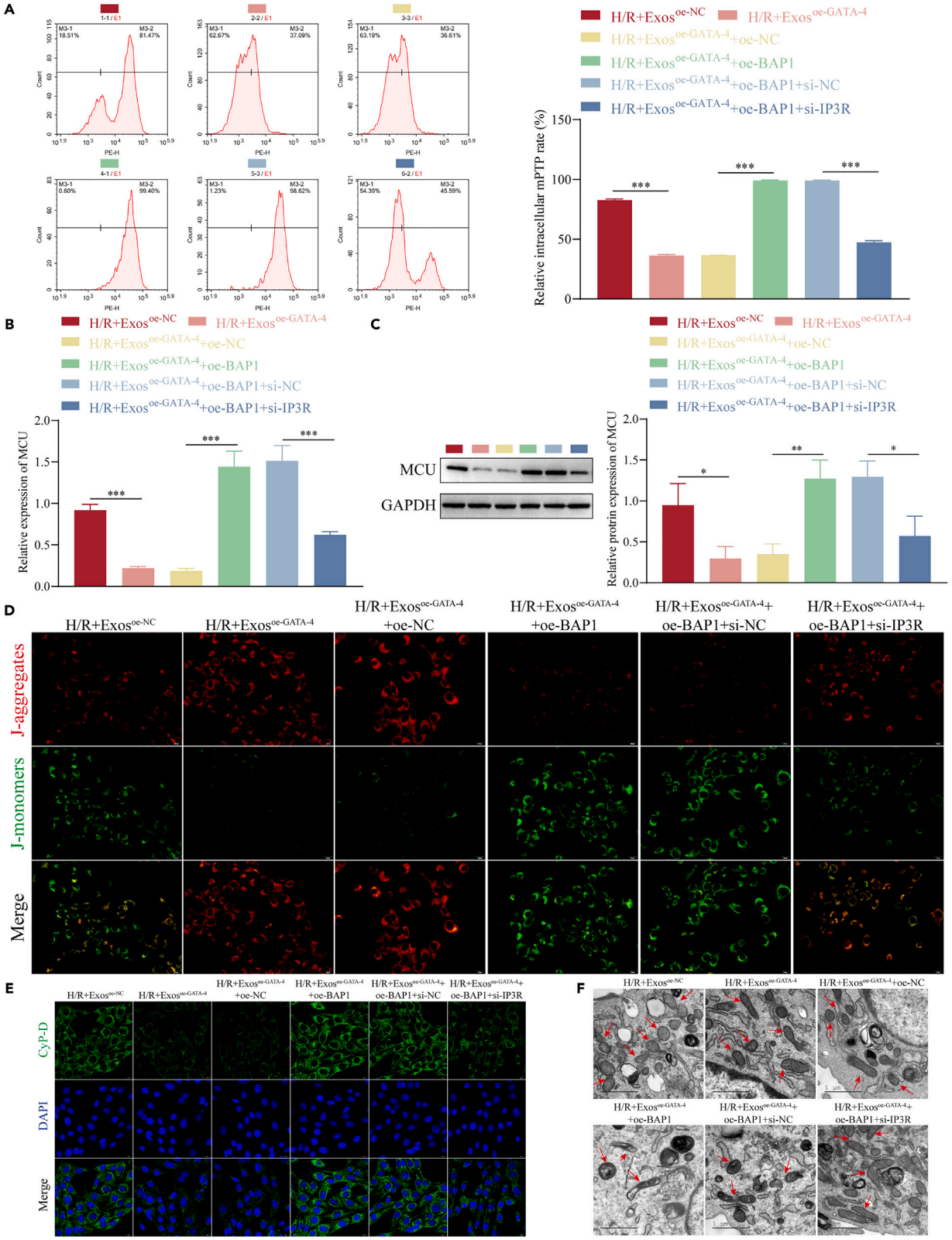
A
1-1 / E1
M3-1 18.51%
M3-2 81.47%
2-2 / E1
M3-1 62.67%
M3-2 37.09%
3-3 / E1
M3-1 63.19%
M3-2 36.61%
4-1 / E1
M3-1 0.60%
M3-2 99.40%
5-3 / E1
M3-1 1.23%
M3-2 98.62%
6-2 / E1
M3-1 54.39%
M3-2 45.59%
Count
PE-H
H/R+Exos^oe-NC
H/R+Exos^oe-GATA-4
H/R+Exos^oe-GATA-4+oe-NC
H/R+Exos^oe-GATA-4+oe-BAP1
H/R+Exos^oe-GATA-4+oe-BAP1+si-NC
H/R+Exos^oe-GATA-4+oe-BAP1+si-IP3R
Relative intracellular mPTP rate (%)
150
100
50
0
***
B
Relative expression of MCU
2.0
1.5
1.0
0.5
0.0
C
MCU
GAPDH
Relative protrin expression of MCU
*
**
D
J-aggregates
J-monomers
Merge
E
CyP-D
DAPI
Merge
F
1 μm

Figure 8. BAP1 induces cardiomyocytes Ca^{2+} overload, leading to mPTP activation and mitochondrial dysfunction through interaction with IP3R

(A) mPTP assessment by flow cytometry.

(B and C) The expression level of MCU was detected by RT-qPCR (B) and western blot (C).

(D) Mitochondrial membrane potential assay (scale bar: 20 μm).

(E) IF detected the fluorescence intensity of CyP-D (scale bar: 20 μm).

(F) TEM was reviewed for mitochondrial morphology (scale bar: 1 μm). $n = 3$, $^{*}p < 0.05$, $^{**}p < 0.01$, $^{***}p < 0.001$. Data are represented as mean ± SD.

increased lipid peroxidation and ferroptosis.[10,33] However, our study did not further confirm the specific mechanism of action of BAP1 targeting to negatively regulate SCL7A11 expression, and subsequent studies are needed to further elucidate how BAP1 regulates SCL7A11 through experiments, chromatin immunoprecipitation sequencing (ChIP-seq) analysis, and high-throughput sequencing.

In addition, studies have discovered that the expression level of BAP1 relates to intracellular Ca^{2+} concentrations.[62] The balance of Ca^{2+} intracellular has a crucial role in mitochondrial dysfunction and cell death.[63] The excessive Ca^{2+} levels induce mPTP opening, which is dependent on Ca^{2+}, causing cell death.[64] The mPTP opens during myocardial I/R injury, during which Ca^{2+} rises and the ROS increases. Thus, target mPTP therapies have an important role in cardioprotection.[65] Liu et al. confirmed that IP3R increases the Ca^{2+} level, activates the mPTP opening and mitochondrial dysfunction, and induces the ferroptosis of kidney injury.[66] Interestingly, BAP1 interacts with the IP3R protein[67,68] to regulate Ca^{2+} and cell death, which is also confirmed in our study. In this study, we observed that *BAP1* increased cardiomyocytes' Ca^{2+} level, causing mPTP opening and mitochondrial dysfunction through interactions with IP3R, and reversed the function of $Exos^{oe-GATA-4}$ inhibited H/R-induced cardiomyocytes ferroptosis. Therefore, $Exos^{oe-GATA-4}$ inhibits H/R-induced cardiomyocyte ferroptosis through BAP1, which interacts with IP3R-inhibited mPTP opening. Similarly, Mewton et al. found that infarct size is reduced, and cardiac function is improved after treatment of CsA,[69] which is an mPTP inhibitor. Finally, in the I/R mice model, $Exos^{oe-GATA-4}$ relieved impaired cardiac function, and decreased infarction area inhibited I/R-induced cardiomyocyte ferroptosis by regulating miR-330-3p, BAP1 and IP3R expression levels.

In this study, we further observed the change in H_2S content in the $Exos^{oe-GATA-4}$ group; the H_2S content was decreased during mPTP opening. H_2S has a vital role in H/R-induced cardiomyocyte injury,[37] and Ca^{2+} induces mPTP opening blocked by high levels of H_2S.[38] H_2S production can further reduce lipid peroxide levels and inhibit ferroptosis.[39] In addition, studies have shown that in H_2S regulation of the keap1/Nrf2 signaling pathway in cardiomyocytes, H_2S increases the expression of Nrf2 and simultaneously reduces the expression of keap1.[70] Similarly, in this study, the H_2S content was increased, the expression levels of keap1 were decreased, and Nrf2 was increased in the $Exos^{oe-GATA-4}$ group. H_2S can induce Nrf2 dissociation from Keap1, leading to enhanced Nrf2 nuclear translocation.[71] We further discovered that the expression of Nrf2 was raised in the nucleus. We speculate that Nrf2 enters the nucleus when H_2S content is increased. This is consistent with Li's study, which reported that Nrf2 enters the nucleus after dissociating from keap1 during oxidative stress.[72] The keap1/Nrf2 signaling pathway is the key regulation of ferroptosis.[73] Keap1/Nrf2 is considered an important oxidative stress regulatory pathway for cardiomyocyte damage and relates to ferroptosis.[74] Therefore, our data suggest that $Exos^{oe-GATA-4}$ may regulate the keap1/Nrf2 signaling pathway by releasing H_2S, in turn inhibiting H/R-induced cardiomyocyte ferroptosis.

In summary, our study found that $Exos^{oe-GATA-4}$ suppresses H/R-induced cardiomyocyte ferroptosis through miR-330-3p, which regulates BAP1/SLC7A11/IP3R axis and mitochondrial permeability transition pore opening. In addition, these effects may connect to H_2S regulated the keap1/Nrf2 signaling pathway. Our results had much significance in treating $Exos^{oe-GATA-4}$ in myocardial I/R injury. However, further research still needs to explore the H_2S-mediated keap1/Nrf2 signaling pathway mechanism, and clinical research is needed to confirm our results further.

Conclusions

In this study, we successfully extracted overexpressing GATA-4 BMSC-derived exosome Exos and explored the function and mechanism of the Exos in H/R-induced cardiomyocytes' ferroptosis. These findings showed that $Exos^{oe-GATA-4}$ effectively suppressed H/R-induced cardiomyocytes' ferroptosis through upregulation of miR-330-3p, to target negative regulated the expression of BAP1. BAP1 can regulate the expression of SLC7A11 to affect H/R-induced cardiomyocytes' ferroptosis or interact with IP3R and increase cardiomyocytes' Ca^{2+} level, causing mPTP opening, promoting H/R-induced cardiomyocytes' ferroptosis. Our findings shed light on the potential of $Exos^{oe-GATA-4}$ as a treatment for H/R-induced cardiomyocyte ferroptosis and as an effective target for it.

Limitations of the study

This study did not further confirm the specific mechanism of action of how BAP1 regulates SCL7A11 expression, and subsequent studies are needed to further elucidate through experiments, ChIP-seq analysis, and high-throughput sequencing. Moreover, the results of this study were only confirmed at the cellular and mouse levels, and clinical research is needed to confirm our results further.

RESOURCE AVAILABILITY

Lead contact

Further information and requests for resources and reagents should be directed to and will be fulfilled by the lead contact, Jigang He (chouchou0708@aliyun.com).

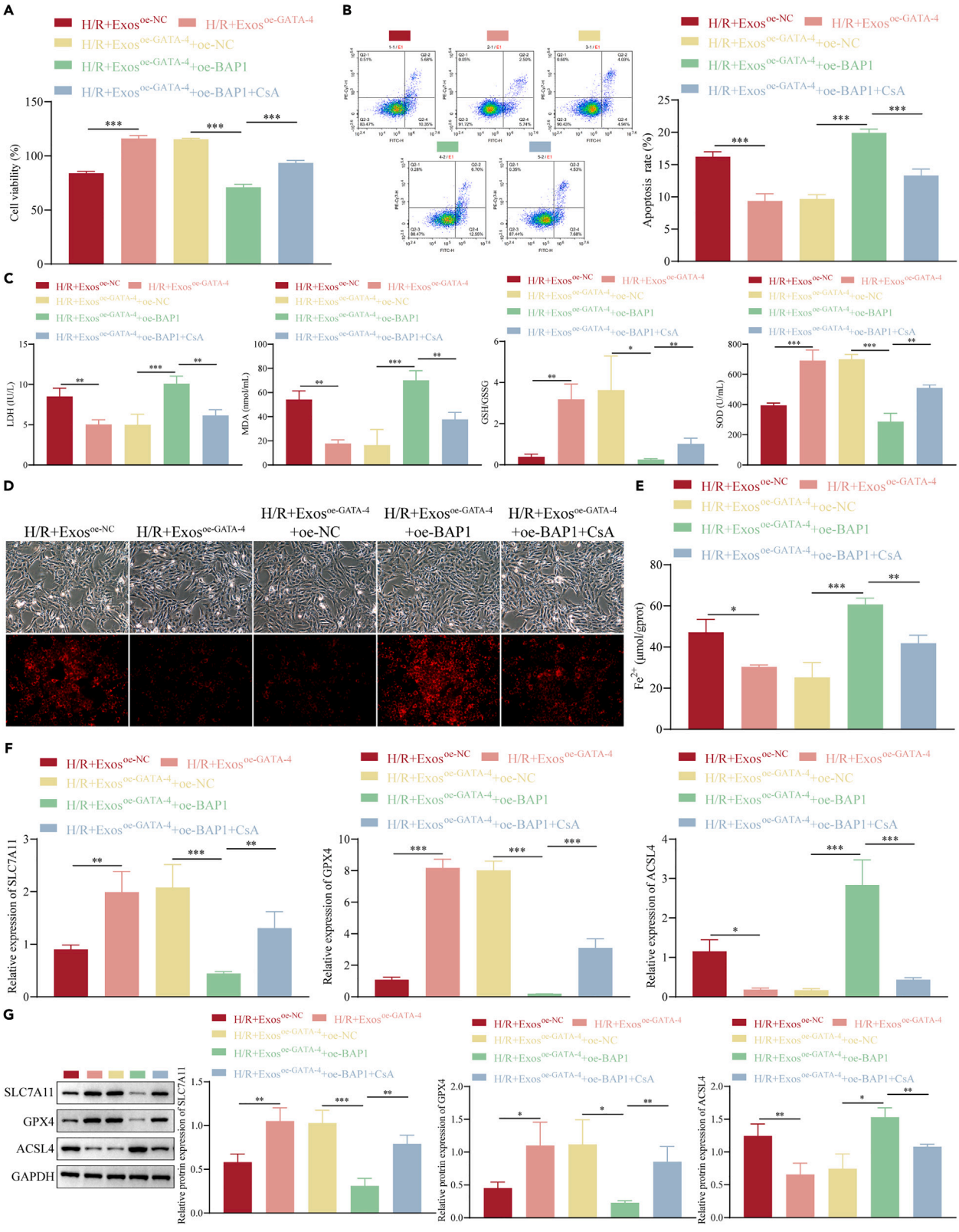
A
H/R+Exos^oe-NC
H/R+Exos^oe-GATA-4
H/R+Exos^oe-GATA-4+oe-NC
H/R+Exos^oe-GATA-4+oe-BAP1
H/R+Exos^oe-GATA-4+oe-BAP1+CsA
Cell viability (%)
B
Apoptosis rate (%)
C
LDH (IU/L)
MDA (nmol/mL)
GSH/GSSG
SOD (U/mL)
D
H/R+Exos^oe-NC
H/R+Exos^oe-GATA-4
H/R+Exos^oe-GATA-4 +oe-NC
H/R+Exos^oe-GATA-4 +oe-BAP1
H/R+Exos^oe-GATA-4 +oe-BAP1+CsA
E
Fe2+ (μmol/gprot)
F
Relative expression of SLC7A11
Relative expression of GPX4
Relative expression of ACSL4
G
SLC7A11
GPX4
ACSL4
GAPDH
Relative protrin expression of SLC7A11
Relative protrin expression of GPX4
Relative protrin expression of ACSL4

Figure 9. BAP1 induces mPTP opening, which reverses the inhibiting role of BMSC-derived Exos$^{oe-GATA-4}$ on H/R-induced cardiomyocyte ferroptosis through interaction with IP3R

(A) CCK-8 assay.

(B) Early and late cell apoptosis detected by flow cytometry.

(C) Levels of LDH, MDA, and GSH were detected by ELISA.

(D and E) The ROS (D) and Fe^{2+} (E) levels were assessed using Kits assay.

(F and G) The expression levels of SLC7A11, GPX4, and ACSL4 were detected by RT-qPCR (F) and western blot (G). $n = 3$, $^{*}p < 0.05$, $^{**}p < 0.01$, $^{***}p < 0.001$. Data are represented as mean ± SD.

Materials availability

This study did not generate new unique reagents.

Data and code availability

- All data produced in this study are included in the published article.
- This work does not report original code.
- Any information needed to re-analyze the data reported in this paper is available upon request from the primary contact.

ACKNOWLEDGMENTS

This work was supported by National Natural Science Foundation of China (No. 82060299), Medical Discipline Leader Project of Yunnan Provincial Health Commission (No. D-2019020), Yunnan Provincial Government Ten Thousand Person-Top Young Talents Project (No. KH-SWR-QNBJ-2019-002), Clinical Medical Center of the First People's Hospital of Yunnan Province (No. 2021LCZXXF-XZ04), Kunming Medical Joint Special Project-Outstanding Youth Cultivation Project (No. 202101AY070001-034), Clinical Medical Center of the First People's Hospital of Yunnan Province (No. 2022LCZXKF-HX05), Kunming Medical joint special project (No. 202101AY070001-272), Famous Doctor Project of "Xingdian Talent Support Plan" of Yunnan Province (No. XDYC-MY-2022-0037), and Yunnan Province 2023 Undergraduate Education and Teaching Reform Research Project (No. 2023BKXJJG-F04002). We are grateful to Yunnan Labreal Biotech Co., Ltd. for their invaluable assistance with the animal experiments. We would like to express our gratitude to MedSci for their assistance with the English language review.

AUTHOR CONTRIBUTIONS

Conceived and designed the experiments, J.H. and Z.X.; performed the experiments, J.H., X.W., and X.C.; analyzed the data, D.Y.; contributed reagents/materials/analysis tools, X.C. and S.L.; writing – original draft, X.W. and J.H.; writing – review & editing, J.H. and Z.X.

DECLARATION OF INTERESTS

All authors declare no competing interests.

STAR★METHODS

Detailed methods are provided in the online version of this paper and include the following:

SUPPLEMENTAL INFORMATION

Supplemental information can be found online at https://doi.org/10.1016/j.isci.2024.110784.

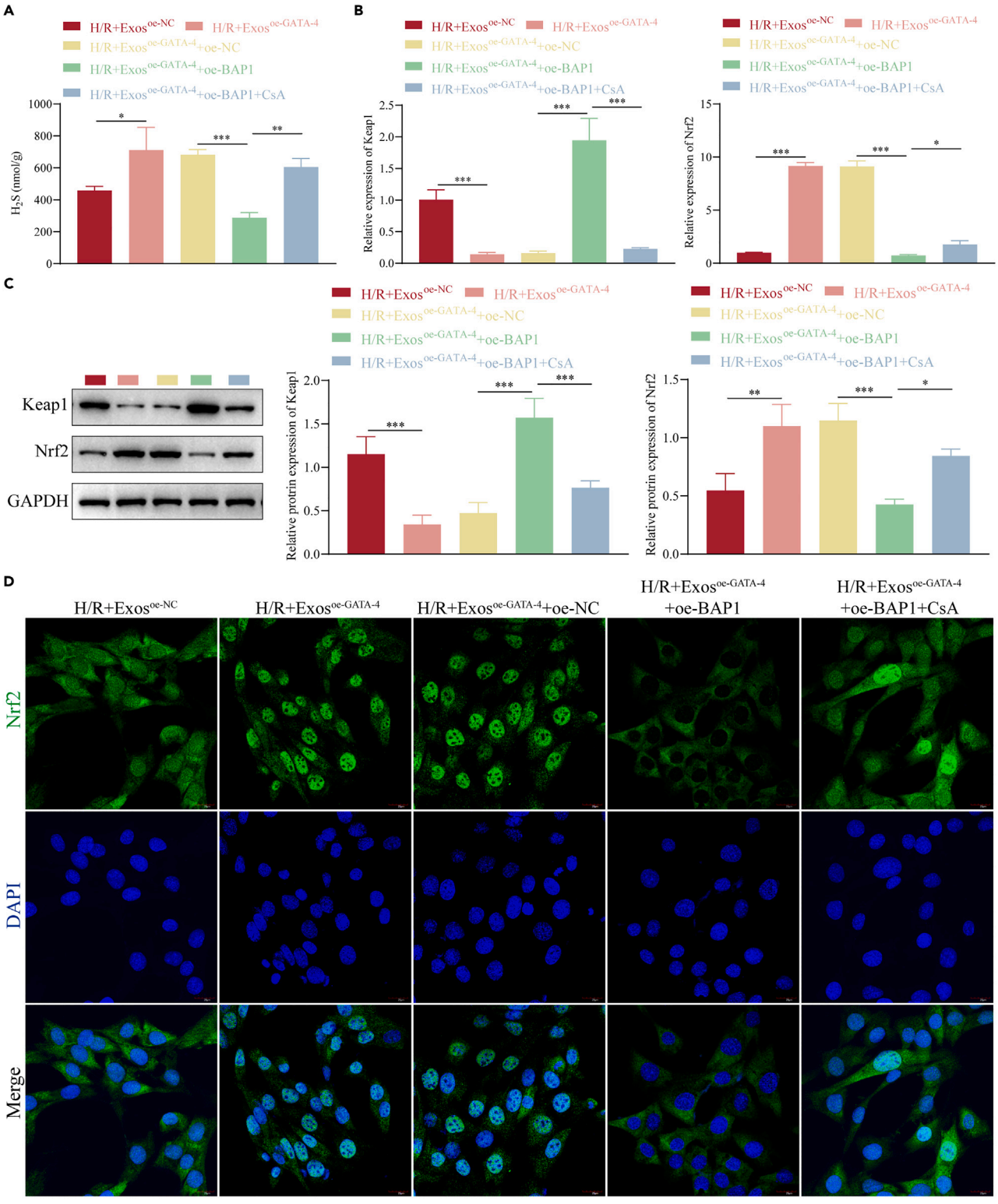

Figure 10. BMSC-derived Exos$^{oe-GATA-4}$ inhibits H/R-induced cardiomyocytes ferroptosis related to keap1/Nrf2 signaling pathway

(A) The content of H_2S was assessed using Kits assay.

(B and C) The expression levels of keap1 and Nrf2 were detected using RT-qPCR (B) and western blot (C).

(D) The expression of Nrf2 was detected using IF (scale bar: 20 μm). $n = 3$, $^*p < 0.05$, $^{**}p < 0.01$, $^{***}p < 0.001$. Data are represented as mean ± SD.

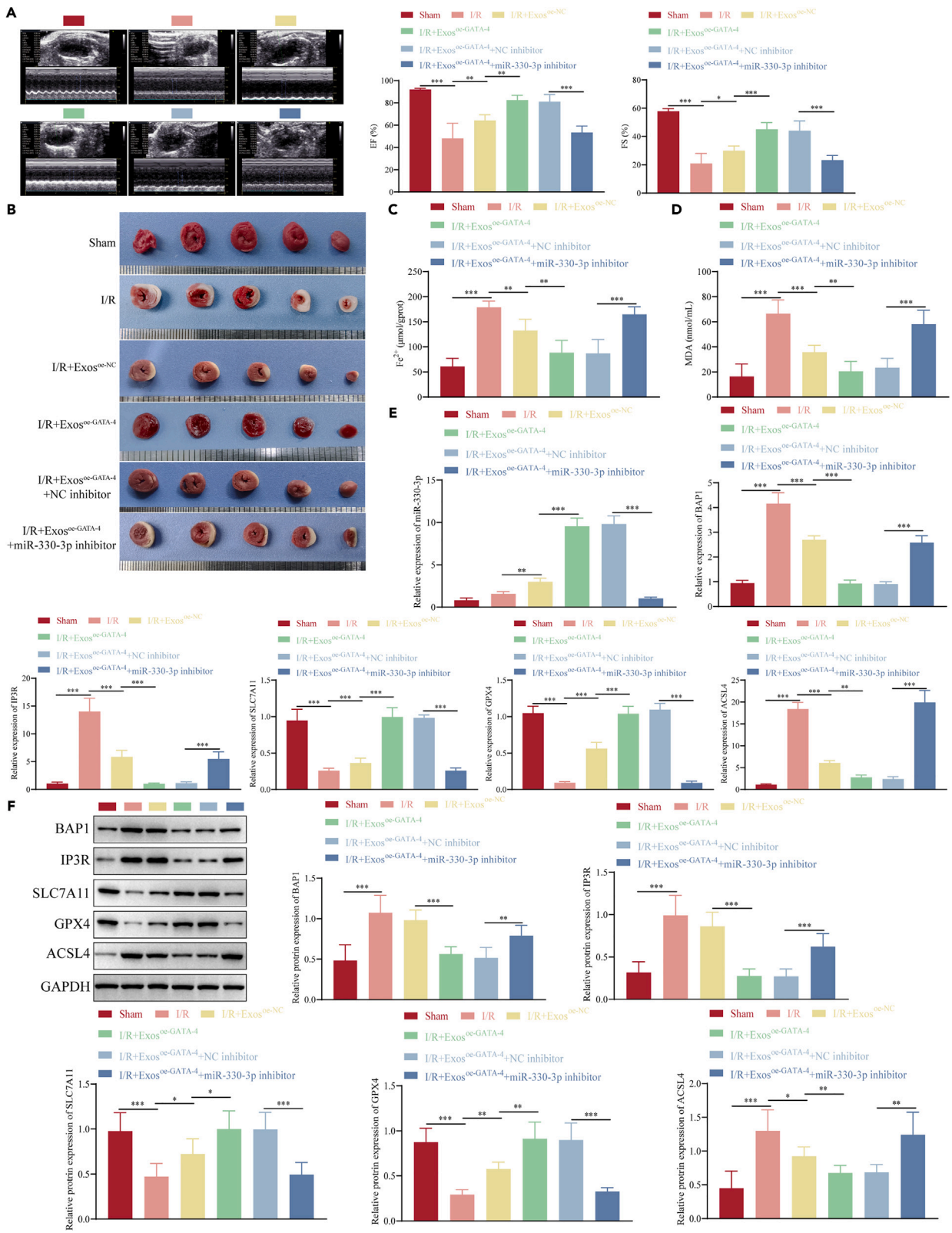
A
B
Sham
I/R
I/R+Exos^oe-NC
I/R+Exos^oe-GATA-4
I/R+Exos^oe-GATA-4 +NC inhibitor
I/R+Exos^oe-GATA-4 +miR-330-3p inhibitor
EF (%)
FS (%)
C
D
E
F
Fe2+ (μmol/gprot)
MDA (nmol/mL)
Relative expression of miR-330-3p
Relative expression of BAP1
Relative expression of IP3R
Relative expression of SLC7A11
Relative expression of GPX4
Relative expression of ACSL4
BAP1
IP3R
SLC7A11
GPX4
ACSL4
GAPDH
Relative protrin expression of BAP1
Relative protrin expression of IP3R
Relative protrin expression of SLC7A11
Relative protrin expression of GPX4
Relative protrin expression of ACSL4

Figure 11. BMSC-derived Exos$^{oe-GATA-4}$ inhibits I/R-induced cardiomyocyte ferroptosis by upregulated miR-330-3p *in vivo*

(A) An ultrasonic cardiogram estimated cardiac function.

(B) The TTC staining.

(C and D) The Fe^{2+} (C) and MDA (D) levels were assessed using Kits assay.

(E) The mRNA expression levels of miR-330-3p, BAP1, IP3R, SLC7A11, GPX4, and ACSL4 were detected by RT-qPCR.

(F) The protein expressions of BAP1, IP3R, SLC7A11, GPX4, and ACSL4 were detected by western blot. $n = 6$, $^*p < 0.05$, $^{**}p < 0.01$, $^{***}p < 0.001$. Data are represented as mean ± SD.

Received: January 30, 2024
Revised: July 1, 2024
Accepted: August 19, 2024
Published: August 22, 2024

REFERENCES

1. Agüero, F., Marrugat, J., Elosua, R., Sala, J., Masiá, R., Ramos, R., and Grau, M.; REGICOR Investigators (2015). New myocardial infarction definition affects incidence, mortality, hospitalization rates and prognosis. Eur. J. Prev. Cardiol. *22*, 1272–1280. https://doi.org/10.1177/2047487314546988.
2. Chi, H.J., Chen, M.L., Yang, X.C., Lin, X.M., Sun, H., Zhao, W.S., Qi, D., Dong, J.L., and Cai, J. (2017). Progress in Therapies for Myocardial Ischemia Reperfusion Injury. Curr. Drug Targets *18*, 1712–1721. https://doi.org/10.2174/1389450117666160401120308.
3. Braunwald, E. (2012). The treatment of acute myocardial infarction: the Past, the Present, and the Future. Eur. Heart J. Acute Cardiovasc. Care *1*, 9–12. https://doi.org/10.1177/2048872612438026.
4. Shen, S., Wang, Z., Sun, H., and Ma, L. (2022). Role of NLRP3 Inflammasome in Myocardial Ischemia-Reperfusion Injury and Ventricular Remodeling. Med. Sci. Mon. Int. Med. J. Exp. Clin. Res. *28*, e934255. https://doi.org/10.12659/msm.934255.
5. Li, J., Cao, F., Yin, H.L., Huang, Z.J., Lin, Z.T., Mao, N., Sun, B., and Wang, G. (2020). Ferroptosis: past, present and future. Cell Death Dis. *11*, 88. https://doi.org/10.1038/s41419-020-2298-2.
6. Li, W., Li, W., Leng, Y., Xiong, Y., and Xia, Z. (2020). Ferroptosis Is Involved in Diabetes Myocardial Ischemia/Reperfusion Injury Through Endoplasmic Reticulum Stress. DNA Cell Biol. *39*, 210–225. https://doi.org/10.1089/dna.2019.5097.
7. Kajarabille, N., and Latunde-Dada, G.O. (2019). Programmed Cell-Death by Ferroptosis: Antioxidants as Mitigators. Int. J. Mol. Sci. *20*, 4968. https://doi.org/10.3390/ijms20194968.
8. Dixon, S.J., Lemberg, K.M., Lamprecht, M.R., Skouta, R., Zaitsev, E.M., Gleason, C.E., Patel, D.N., Bauer, A.J., Cantley, A.M., Yang, W.S., et al. (2012). Ferroptosis: an iron-dependent form of nonapoptotic cell death. Cell *149*, 1060–1072. https://doi.org/10.1016/j.cell.2012.03.042.
9. Hu, K., Li, K., Lv, J., Feng, J., Chen, J., Wu, H., Cheng, F., Jiang, W., Wang, J., Pei, H., et al. (2020). Suppression of the SLC7A11/glutathione axis causes synthetic lethality in KRAS-mutant lung adenocarcinoma. J. Clin. Invest. *130*, 1752–1766. https://doi.org/10.1172/jci124049.
10. Zhang, Y., Shi, J., Liu, X., Feng, L., Gong, Z., Koppula, P., Sirohi, K., Li, X., Wei, Y., Lee, H., et al. (2018). BAP1 links metabolic regulation of ferroptosis to tumour suppression. Nat. Cell Biol. *20*, 1181–1192. https://doi.org/10.1038/s41556-018-0178-0.
11. Golpanian, S., Wolf, A., Hatzistergos, K.E., and Hare, J.M. (2016). Rebuilding the Damaged Heart: Mesenchymal Stem Cells, Cell-Based Therapy, and Engineered Heart Tissue. Physiol. Rev. *96*, 1127–1168. https://doi.org/10.1152/physrev.00019.2015.
12. Zhang, L.L., Xiong, Y.Y., and Yang, Y.J. (2021). The Vital Roles of Mesenchymal Stem Cells and the Derived Extracellular Vesicles in Promoting Angiogenesis After Acute Myocardial Infarction. Stem Cell. Dev. *30*, 561–577. https://doi.org/10.1089/scd.2021.0006.
13. Zhao, J., Li, X., Hu, J., Chen, F., Qiao, S., Sun, X., Gao, L., Xie, J., and Xu, B. (2019). Mesenchymal stromal cell-derived exosomes attenuate myocardial ischaemia-reperfusion injury through miR-182-regulated macrophage polarization. Cardiovasc. Res. *115*, 1205–1216. https://doi.org/10.1093/cvr/cvz040.
14. Gao, L., Qiu, F., Cao, H., Li, H., Dai, G., Ma, T., Gong, Y., Luo, W., Zhu, D., Qiu, Z., et al. (2023). Therapeutic delivery of microRNA-125a-5p oligonucleotides improves recovery from myocardial ischemia/reperfusion injury in mice and swine. Theranostics *13*, 685–703. https://doi.org/10.7150/thno.73568.
15. Gan, B. (2021). Mitochondrial regulation of ferroptosis. J. Cell Biol. *220*, e202105043. https://doi.org/10.1083/jcb.202105043.
16. Gogvadze, V., Walter, P.B., and Ames, B.N. (2003). The role of Fe2+-induced lipid peroxidation in the initiation of the mitochondrial permeability transition. Arch. Biochem. Biophys. *414*, 255–260. https://doi.org/10.1016/s0003-9861(02)00750-6.
17. Petrosillo, G., Colantuono, G., Moro, N., Ruggiero, F.M., Tiravanti, E., Di Venosa, N., Fiore, T., and Paradies, G. (2009). Melatonin protects against heart ischemia-reperfusion injury by inhibiting mitochondrial permeability transition pore opening. Am. J. Physiol. Heart Circ. Physiol. *297*, H1487–H1493. https://doi.org/10.1152/ajpheart.00163.2009.
18. Di Lisa, F., Menabò, R., Canton, M., Barile, M., and Bernardi, P. (2001). Opening of the mitochondrial permeability transition pore causes depletion of mitochondrial and cytosolic NAD+ and is a causative event in the death of myocytes in postischemic reperfusion of the heart. J. Biol. Chem. *276*, 2571–2575. https://doi.org/10.1074/jbc.M006825200.
19. Luongo, T.S., Lambert, J.P., Gross, P., Nwokedi, M., Lombardi, A.A., Shanmughapriya, S., Carpenter, A.C., Kolmetzky, D., Gao, E., van Berlo, J.H., et al. (2017). The mitochondrial Na(+)/Ca(2+) exchanger is essential for Ca(2+) homeostasis and viability. Nature *545*, 93–97. https://doi.org/10.1038/nature22082.
20. Wei, S., Qiu, T., Yao, X., Wang, N., Jiang, L., Jia, X., Tao, Y., Wang, Z., Pei, P., Zhang, J., et al. (2020). Arsenic induces pancreatic dysfunction and ferroptosis via mitochondrial ROS-autophagy-lysosomal pathway. J. Hazard Mater. *384*, 121390. https://doi.org/10.1016/j.jhazmat.2019.121390.
21. Triantafilou, K., Hughes, T.R., Triantafilou, M., and Morgan, B.P. (2013). The complement membrane attack complex triggers intracellular Ca2+ fluxes leading to NLRP3 inflammasome activation. J. Cell Sci. *126*, 2903–2913. https://doi.org/10.1242/jcs.124388.
22. Rossi, A., Pizzo, P., and Filadi, R. (2019). Calcium, mitochondria and cell metabolism: A functional triangle in bioenergetics. Biochim. Biophys. Acta Mol. Cell Res. *1866*, 1068–1078. https://doi.org/10.1016/j.bbamcr.2018.10.016.
23. Cheng, Y., Zhu, H., and Gao, W. (2020). MicroRNA-330-3p represses the proliferation and invasion of laryngeal squamous cell carcinoma through downregulation of Tra2β-mediated Akt signaling. Mol. Cell. Probes *52*, 101574. https://doi.org/10.1016/j.mcp.2020.101574.
24. Guan, A., Wang, H., Li, X., Xie, H., Wang, R., Zhu, Y., and Li, R. (2016). MiR-330-3p inhibits gastric cancer progression through targeting MSI1. Am. J. Transl. Res. *8*, 4802–4811.
25. Cai, L., Ye, L., Hu, X., He, W., Zhuang, D., Guo, Q., Shu, K., and Jie, Y. (2021). MicroRNA miR-330-3p suppresses the progression of ovarian cancer by targeting RIPK4. Bioengineered *12*, 440–449. https://doi.org/10.1080/21655979.2021.1871817.
26. He, J.G., Li, H.R., Han, J.X., Li, B.B., Yan, D., Li, H.Y., Wang, P., and Luo, Y. (2018). GATA-4-expressing mouse bone marrow mesenchymal stem cells improve cardiac function after myocardial infarction via secreted exosomes. Sci. Rep. *8*, 9047. https://doi.org/10.1038/s41598-018-27435-9.
27. Mesci, A., Huang, X., Taeb, S., Jahangiri, S., Kim, Y., Fokas, E., Bruce, J., Leong, H.S., and Liu, S.K. (2017). Targeting of CCBE1 by miR-330-3p in human breast cancer promotes metastasis. Br. J. Cancer *116*, 1350–1357. https://doi.org/10.1038/bjc.2017.105.
28. Yang, C., Mou, Z., Zhang, Z., Wu, S., Zhou, Q., Chen, Y., Gong, J., Xu, C., Ou, Y., Chen, X., et al. (2021). Circular RNA RBPMS inhibits

bladder cancer progression via miR-330-3p/RAI2 regulation. Mol. Ther. Nucleic Acids *23*, 872–886. https://doi.org/10.1016/j.omtn.2021.01.009.

29. Hou, R., Guo, D., Fan, M., Hou, Y., Zhao, J., and Wu, X. (2022). Screening and Analysis of Potential Critical Gene in Acute Myocardial Infarction Based on a miRNA-mRNA Regulatory Network. Int. J. Gen. Med. *15*, 2847–2860. https://doi.org/10.2147/ijgm.S354641.
30. Sun, X.L., Zhang, Y.L., Xi, S.M., Ma, L.J., and Li, S.P. (2019). MiR-330-3p suppresses phosphoglycerate mutase family member 5 -inducted mitophagy to alleviate hepatic ischemia-reperfusion injury. J. Cell. Biochem. *120*, 4255–4267. https://doi.org/10.1002/jcb.27711.
31. Liu, H., Mo, H., Yang, C., Mei, X., Song, X., Lu, W., Xiao, H., Yan, J., Wang, X., Yan, J., et al. (2022). A novel function of ATF3 in suppression of ferroptosis in mouse heart suffered ischemia/reperfusion. Free Radic. Biol. Med. *189*, 122–135. https://doi.org/10.1016/j.freeradbiomed.2022.07.006.
32. Yan, Y.C., Meng, G.X., Ding, Z.N., Liu, Y.F., Chen, Z.Q., Yan, L.J., Yang, Y.F., Liu, H., Yang, C.C., Dong, Z.R., et al. (2022). Somatic mutation and expression of BAP1 in hepatocellular carcinoma: an indicator for ferroptosis and immune checkpoint inhibitor therapies. J. Cancer *13*, 88–101. https://doi.org/10.7150/jca.65574.
33. Zhang, Y., Koppula, P., and Gan, B. (2019). Regulation of H2A ubiquitination and SLC7A11 expression by BAP1 and PRC1. Cell Cycle *18*, 773–783. https://doi.org/10.1080/15384101.2019.1597506.
34. Sanada, S., Komuro, I., and Kitakaze, M. (2011). Pathophysiology of myocardial reperfusion injury: preconditioning, postconditioning, and translational aspects of protective measures. Am. J. Physiol. Heart Circ. Physiol. *301*, H1723–H1741. https://doi.org/10.1152/ajpheart.00553.2011.
35. Kim, J.S., Wang, J.H., and Lemasters, J.J. (2012). Mitochondrial permeability transition in rat hepatocytes after anoxia/reoxygenation: role of Ca2+-dependent mitochondrial formation of reactive oxygen species. Am. J. Physiol. Gastrointest. Liver Physiol. *302*, G723–G731. https://doi.org/10.1152/ajpgi.00082.2011.
36. Filadi, R., Basso, E., Lefkimmiatis, K., and Pozzan, T. (2017). Beyond Intracellular Signaling: The Ins and Outs of Second Messengers Microdomains. Adv. Exp. Med. Biol. *981*, 279–322. https://doi.org/10.1007/978-3-319-55858-5_12.
37. Li, H., Zhang, C., Sun, W., Li, L., Wu, B., Bai, S., Li, H., Zhong, X., Wang, R., Wu, L., and Xu, C. (2015). Exogenous hydrogen sulfide restores cardioprotection of ischemic post-conditioning via inhibition of mPTP opening in the aging cardiomyocytes. Cell Biosci. *5*, 43. https://doi.org/10.1186/s13578-015-0035-9.
38. Papu John, A.S., Kundu, S., Pushpakumar, S., Amin, M., Tyagi, S.C., and Sen, U. (2019). Hydrogen sulfide inhibits Ca(2+)-induced mitochondrial permeability transition pore opening in type-1 diabetes. Am. J. Physiol. Endocrinol. Metab. *317*, E269–E283. https://doi.org/10.1152/ajpendo.00251.2018.
39. Miao, Y., Zhang, S., Liang, Z., Wang, Y., Tian, D., Jin, S., Guo, Q., Xue, H., Teng, X., Xiao, L., and Wu, Y. (2023). Hydrogen sulfide ameliorates endothelial dysfunction in aging arteries by regulating ferroptosis. Nitric Oxide *140–141*, 77–90. https://doi.org/10.1016/j.niox.2023.10.002.
40. Zhang, H., Pan, J., Huang, S., Chen, X., Chang, A.C.Y., Wang, C., Zhang, J., and Zhang, H. (2024). Hydrogen sulfide protects cardiomyocytes from doxorubicin-induced ferroptosis through the SLC7A11/GSH/GPx4 pathway by Keap1 S-sulfhydration and Nrf2 activation. Redox Biol. *70*, 103066. https://doi.org/10.1016/j.redox.2024.103066.
41. Katsaraki, K., Karousi, P., Artemaki, P.I., Scorilas, A., Pappa, V., Kontos, C.K., and Papageorgiou, S.G. (2021). MicroRNAs: Tiny Regulators of Gene Expression with Pivotal Roles in Normal B-Cell Development and B-Cell Chronic Lymphocytic Leukemia. Cancers *13*, 593. https://doi.org/10.3390/cancers13040593.
42. Nakamura, Y., Miyaki, S., Ishitobi, H., Matsuyama, S., Nakasa, T., Kamei, N., Akimoto, T., Higashi, Y., and Ochi, M. (2015). Mesenchymal-stem-cell-derived exosomes accelerate skeletal muscle regeneration. FEBS Lett. *589*, 1257–1265. https://doi.org/10.1016/j.febslet.2015.03.031.
43. Zhang, X., Sai, B., Wang, F., Wang, L., Wang, Y., Zheng, L., Li, G., Tang, J., and Xiang, J. (2019). Hypoxic BMSC-derived exosomal miRNAs promote metastasis of lung cancer cells via STAT3-induced EMT. Mol. Cancer *18*, 40. https://doi.org/10.1186/s12943-019-0959-5.
44. Liu, J., Huang, L., Zhu, Y., He, Y., Zhang, W., Lei, T., Xuan, J., Xiao, B., Li, L., Zhou, Q., and Sun, Z. (2021). Exploring the Expression and Prognostic Value of the TCP1 Ring Complex in Hepatocellular Carcinoma and Overexpressing Its Subunit 5 Promotes HCC Tumorigenesis. Front. Oncol. *11*, 739660. https://doi.org/10.3389/fonc.2021.739660.
45. Mao, S., Zhao, J., Zhang, Z.J., and Zhao, Q. (2022). MiR-183-5p overexpression in bone mesenchymal stem cell-derived exosomes protects against myocardial ischemia/reperfusion injury by targeting FOXO1. Immunobiology *227*, 152204. https://doi.org/10.1016/j.imbio.2022.152204.
46. Dalton, S., Smith, K., Singh, K., Kaiser, H., Kolhe, R., Mondal, A.K., Khayrullin, A., Isales, C.M., Hamrick, M.W., Hill, W.D., and Fulzele, S. (2020). Accumulation of kynurenine elevates oxidative stress and alters microRNA profile in human bone marrow stromal cells. Exp. Gerontol. *130*, 110800. https://doi.org/10.1016/j.exger.2019.110800.
47. Yi, F., Xiao, H., Song, M., Huang, L., Huang, Q., Deng, J., Yang, H., Zheng, L., Wang, H., and Gu, W. (2024). BMSC-derived exosomal miR-148b-3p attenuates OGD/R-induced HMC3 cell activation by targeting DLL4 and Notch1. Neurosci. Res. *199*, 36–47. https://doi.org/10.1016/j.neures.2023.09.005.
48. Chen, Y., Liu, H., Zou, J., Cao, G., Li, Y., Xing, C., and Wu, J. (2023). Exosomal circ_0091741 promotes gastric cancer cell autophagy and chemoresistance via the miR-330-3p/TRIM14/Dvl2/Wnt/β-catenin axis. Hum. Cell *36*, 258–275. https://doi.org/10.1007/s13577-022-00790-6.
49. Lawson, A., Snyder, W., and Peeples, E.S. (2022). Intranasal Administration of Extracellular Vesicles Mitigates Apoptosis in a Mouse Model of Neonatal Hypoxic-Ischemic Brain Injury. Neonatology *119*, 345–353. https://doi.org/10.1159/000522644.
50. Chen, Y.R., and Zweier, J.L. (2014). Cardiac mitochondria and reactive oxygen species generation. Circ. Res. *114*, 524–537. https://doi.org/10.1161/circresaha.114.300559.
51. Kagan, V.E., Mao, G., Qu, F., Angeli, J.P.F., Doll, S., Croix, C.S., Dar, H.H., Liu, B., Tyurin, V.A., Ritov, V.B., et al. (2017). Oxidized arachidonic and adrenic PEs navigate cells to ferroptosis. Nat. Chem. Biol. *13*, 81–90. https://doi.org/10.1038/nchembio.2238.
52. Tan, M., Yin, Y., Ma, X., Zhang, J., Pan, W., Tan, M., Zhao, Y., Yang, T., Jiang, T., and Li, H. (2023). Glutathione system enhancement for cardiac protection: pharmacological options against oxidative stress and ferroptosis. Cell Death Dis. *14*, 131. https://doi.org/10.1038/s41419-023-05645-y.
53. Jang, S., Chapa-Dubocq, X.R., Tyurina, Y.Y., St Croix, C.M., Kapralov, A.A., Tyurin, V.A., Bayır, H., Kagan, V.E., and Javadov, S. (2021). Elucidating the contribution of mitochondrial glutathione to ferroptosis in cardiomyocytes. Redox Biol. *45*, 102021. https://doi.org/10.1016/j.redox.2021.102021.
54. Wang, H., Liu, G., Li, T., Wang, N., Wu, J., and Zhi, H. (2020). MiR-330-3p functions as a tumor suppressor that regulates glioma cell proliferation and migration by targeting CELF1. Arch. Med. Sci. *16*, 1166–1175. https://doi.org/10.5114/aoms.2020.95027.
55. Wei, C., Zhang, R., Cai, Q., Gao, X., Tong, F., Dong, J., Hu, Y., Wu, G., and Dong, X. (2019). MicroRNA-330-3p promotes brain metastasis and epithelial-mesenchymal transition via GRIA3 in non-small cell lung cancer. Aging *11*, 6734–6761. https://doi.org/10.18632/aging.102201.
56. Han, A., Purwin, T.J., and Aplin, A.E. (2021). Roles of the BAP1 Tumor Suppressor in Cell Metabolism. Cancer Res. *81*, 2807–2814. https://doi.org/10.1158/0008-5472.Can-20-3430.
57. Baas, R., J van der Wal, F., Bleijerveld, O.B., van Attikum, H., and Sixma, T.K. (2021). Proteomic analysis identifies novel binding partners of BAP1. PLoS One *16*, e0257688. https://doi.org/10.1371/journal.pone.0257688.
58. Jiang, L., Kon, N., Li, T., Wang, S.J., Su, T., Hibshoosh, H., Baer, R., and Gu, W. (2015). Ferroptosis as a p53-mediated activity during tumour suppression. Nature *520*, 57–62. https://doi.org/10.1038/nature14344.
59. Yadav, P., Sharma, P., Sundaram, S., Venkatraman, G., Bera, A.K., and Karunagaran, D. (2021). SLC7A11/xCT is a target of miR-5096 and its restoration partially rescues miR-5096-mediated ferroptosis and anti-tumor effects in human breast cancer cells. Cancer Lett. *522*, 211–224. https://doi.org/10.1016/j.canlet.2021.09.033.
60. Zhang, L., Liu, W., Liu, F., Wang, Q., Song, M., Yu, Q., Tang, K., Teng, T., Wu, D., Wang, X., et al. (2020). IMCA Induces Ferroptosis Mediated by SLC7A11 through the AMPK/mTOR Pathway in Colorectal Cancer. Oxid. Med. Cell. Longev. *2020*, 1675613. https://doi.org/10.1155/2020/1675613.
61. Fang, X., Cai, Z., Wang, H., Han, D., Cheng, Q., Zhang, P., Gao, F., Yu, Y., Song, Z., Wu, Q., et al. (2020). Loss of Cardiac Ferritin H Facilitates Cardiomyopathy via Slc7a11-Mediated Ferroptosis. Circ. Res. *127*, 486–501. https://doi.org/10.1161/circresaha.120.316509.
62. Bononi, A., Giorgi, C., Patergnani, S., Larson, D., Verbruggen, K., Tanji, M., Pellegrini, L., Signorato, V., Olivetto, F., Pastorino, S., et al. (2017). BAP1 regulates IP3R3-mediated Ca(2+) flux to mitochondria suppressing cell transformation. Nature *546*, 549–553. https://doi.org/10.1038/nature22798.

63. Butler, M.R., Ma, H., Yang, F., Belcher, J., Le, Y.Z., Mikoshiba, K., Biel, M., Michalakis, S., Iuso, A., Križaj, D., and Ding, X.Q. (2017). Endoplasmic reticulum (ER) Ca(2+)-channel activity contributes to ER stress and cone death in cyclic nucleotide-gated channel deficiency. J. Biol. Chem. *292*, 11189–11205. https://doi.org/10.1074/jbc.M117.782326.
64. Bernardi, P., Gerle, C., Halestrap, A.P., Jonas, E.A., Karch, J., Mnatsakanyan, N., Pavlov, E., Sheu, S.S., and Soukas, A.A. (2023). Identity, structure, and function of the mitochondrial permeability transition pore: controversies, consensus, recent advances, and future directions. Cell Death Differ. *30*, 1869–1885. https://doi.org/10.1038/s41418-023-01187-0.
65. Murphy, E., and Steenbergen, C. (2008). Mechanisms underlying acute protection from cardiac ischemia-reperfusion injury. Physiol. Rev. *88*, 581–609. https://doi.org/10.1152/physrev.00024.2007.
66. Liu, Z., Ma, J., Zuo, X., Zhang, X., Xie, H., Wang, F., Wu, C., Zhang, J., and Zhu, Q. (2023). IP3R-dependent mitochondrial dysfunction mediates C5b-9-induced ferroptosis in trichloroethylene-caused immune kidney injury. Front. Immunol. *14*, 1106693. https://doi.org/10.3389/fimmu.2023.1106693.
67. Ye, Y., Li, X., Feng, G., Ma, Y., Ye, F., Shen, H., Sun, K., Lu, R., and Miao, S. (2022). 3,3′-Diindolylmethane induces ferroptosis by BAP1-IP3R axis in BGC-823 gastric cancer cells. Anti Cancer Drugs *33*, 362–370. https://doi.org/10.1097/cad.0000000000001270.
68. Ando, H., Kawaai, K., Bonneau, B., and Mikoshiba, K. (2018). Remodeling of Ca(2+) signaling in cancer: Regulation of inositol 1,4,5-trisphosphate receptors through oncogenes and tumor suppressors. Adv. Biol. Regul. *68*, 64–76. https://doi.org/10.1016/j.jbior.2017.12.001.
69. Mewton, N., Croisille, P., Gahide, G., Rioufol, G., Bonnefoy, E., Sanchez, I., Cung, T.T., Sportouch, C., Angoulvant, D., Finet, G., et al. (2010). Effect of cyclosporine on left ventricular remodeling after reperfused myocardial infarction. J. Am. Coll. Cardiol. *55*, 1200–1205. https://doi.org/10.1016/j.jacc.2009.10.052.
70. Li, Y., Chandra, T.P., Song, X., Nie, L., Liu, M., Yi, J., Zheng, X., Chu, C., and Yang, J. (2021). H2S improves doxorubicin-induced myocardial fibrosis by inhibiting oxidative stress and apoptosis via Keap1-Nrf2. Technol. Health Care *29*, 195–209. https://doi.org/10.3233/thc-218020.
71. Yang, G., Zhao, K., Ju, Y., Mani, S., Cao, Q., Puukila, S., Khaper, N., Wu, L., and Wang, R. (2013). Hydrogen sulfide protects against cellular senescence via S-sulfhydration of Keap1 and activation of Nrf2. Antioxidants Redox Signal. *18*, 1906–1919. https://doi.org/10.1089/ars.2012.4645.
72. Li, S., Shi, M., Wang, Y., Xiao, Y., Cai, D., and Xiao, F. (2021). Keap1-Nrf2 pathway up-regulation via hydrogen sulfide mitigates polystyrene microplastics induced-hepatotoxic effects. J. Hazard Mater. *402*, 123933. https://doi.org/10.1016/j.jhazmat.2020.123933.
73. Shen, K., Wang, X., Wang, Y., Jia, Y., Zhang, Y., Wang, K., Luo, L., Cai, W., Li, J., Li, S., et al. (2023). miR-125b-5p in adipose derived stem cells exosome alleviates pulmonary microvascular endothelial cells ferroptosis via Keap1/Nrf2/GPX4 in sepsis lung injury. Redox Biol. *62*, 102655. https://doi.org/10.1016/j.redox.2023.102655.
74. Hou, K., Shen, J., Yan, J., Zhai, C., Zhang, J., Pan, J.A., Zhang, Y., Jiang, Y., Wang, Y., Lin, R.Z., et al. (2021). Loss of TRIM21 alleviates cardiotoxicity by suppressing ferroptosis induced by the chemotherapeutic agent doxorubicin. EBioMedicine *69*, 103456. https://doi.org/10.1016/j.ebiom.2021.103456.
75. Meirelles, L.d.S., and Nardi, N.B. (2003). Murine marrow-derived mesenchymal stem cell: isolation, in vitro expansion, and characterization. Br. J. Haematol. *123*, 702–711. https://doi.org/10.1046/j.1365-2141.2003.04669.x.
76. Ulusan Bağcı, Ö., and Caner, A. (2021). [Defining the Molecular Signal Pathways and Upstream Regulators in Cutaneous Leishmaniasis with Transcriptomic Data Approach]. Mikrobiyoloji Bulteni *55*, 67–80. https://doi.org/10.5578/mb.20092.
77. Yao, H., Xie, Q., He, Q., Zeng, L., Long, J., Gong, Y., Li, X., Li, X., Liu, W., Xu, Z., et al. (2022). Pretreatment with Panaxatriol Saponin Attenuates Mitochondrial Apoptosis and Oxidative Stress to Facilitate Treatment of Myocardial Ischemia-Reperfusion Injury via the Regulation of Keap1/Nrf2 Activity. Oxid. Med. Cell. Longev. *2022*, 9626703. https://doi.org/10.1155/2022/9626703.
78. Cui, Z., He, J., Zhu, J., Ni, W., Liu, L., Bian, Z., Mao, S., Gu, S., Shan, Y., Chu, Z., et al. (2023). O-GlcNAcylated LARP1 positively regulated by circCLNS1A facilitates hepatoblastoma progression through DKK4/β-catenin signalling. Clin. Transl. Med. *13*, e1239. https://doi.org/10.1002/ctm2.1239.
79. Du, W.W., Yang, W., Liu, E., Yang, Z., Dhaliwal, P., and Yang, B.B. (2016). Foxo3 circular RNA retards cell cycle progression via forming ternary complexes with p21 and CDK2. Nucleic Acids Res. *44*, 2846–2858. https://doi.org/10.1093/nar/gkw027.
80. Zhou, L.Y., Zhai, M., Huang, Y., Xu, S., An, T., Wang, Y.H., Zhang, R.C., Liu, C.Y., Dong, Y.H., Wang, M., et al. (2019). The circular RNA ACR attenuates myocardial ischemia/reperfusion injury by suppressing autophagy via modulation of the Pink1/FAM65B pathway. Cell Death Differ. *26*, 1299–1315. https://doi.org/10.1038/s41418-018-0206-4.

STAR★METHODS

KEY RESOURCES TABLE

REAGENT or RESOURCE	SOURCE	IDENTIFIER
Antibodies		
anti-SLC7A11	Abcam	ab175186; RRID : AB_2722749
anti-GPX4	Abcam	ab125066; RRID : AB_10973901
anti-ACSL4	Abcam	ab155282; RRID : AB_2714020
anti-BAP1	Abcam	ab255611
anti-Keap1	bioss	bs-3648R; RRID : AB_10856809
anti-Nrf2	bioss	bs-1074R; RRID : AB_10855421
anti-IP3R	Abcam	ab252536
anti-MCU	MedChemExpress	HY-P80216
anti-HIF-1α	Abcam	ab179483; RRID : AB_2732807
anti-Bcl-2	Abcam	ab182858; RRID : AB_2715467
anti-Bax	Abcam	ab32503; RRID : AB_725631
antibodies conjugated with HRP	Abcam	ab205718; RRID : AB_2819160
β-actin	Abcam	ab8226; RRID : AB_306371
GAPDH	Abcam	ab9485; RRID : AB_570852
anti-CyP-D	Abcam	ab110324; RRID : AB_10864110
anti-Nrf2	Affinity	BF8017; RRID : AB_3083515
Bacterial and virus strains		
Lentivirus	This paper	N/A
Biological samples		
Cardiac tissue in mice	This paper	N/A
Chemicals, peptides, and recombinant proteins		
Bone marrow mesenchymal stem cell growth medium	Cyagen Biosciences	MUXMX-90011
FBS	Gibco	10099–141
PBS	ZSGB-Bio	ZLI-9061
Lipofectamine 3000 reagent	Invitrogen	L3000150
Cyclosporin A	MedChemExpress	59865-13-3
TRIzol reagent	Invitrogen	15596026
MEM medium	gibco	11095080
Double-antibody	gibco	1902417
SYBR Green PCR Master Mix	ThermoFisher	K0253
RIPA buffer	Sigma-Aldrich	V900854
PVDF membrane	Millipore	IPVH00010
BSA	biofroxx	4240GR100
Critical commercial assays		
mirVana purification miRNA Isolation Kit	Invitrogen	AM1561
TRIzol reagent	Invitrogen	15596026
One Step Prime Script miRNA cDNA Synthesis Kit	Takara	6110A
CCK-8 test kit	Biyuntian	C0037
Annexin-V-FITC/PI apoptosis kit	7seapharmtech	A005-4
LDH assay kit	Enzyme-linked	ml002267

(*Continued on next page*)

Continued

REAGENT or RESOURCE	SOURCE	IDENTIFIER
MDA assay kit	Enzyme-linked	ml077384
GSH assay kit	Enzyme-linked	ml002260
GSSG assay kit	Enzyme-linked	ml057674
SOD assay kit	Enzyme-linked	ml001998
CellROX™ Deep Red kit	ThermoFisher	C10422
Ferrous Ion Content Assay Kit	Solarbio	BC5415
Fluo-8 calcium flux assay kit	Abcam	ab112129
H_2S content Assay Kit	Solarbio	BC2055
mPTP assay kit	Beyotime	C2009S
JC-1 Mitochondrial Membrane Potential Assay Kit	MedChemExpress	HY-K0601
Dual luciferase assay kit	Biyuntian	RG027
Magna RIP™ RNA-Binding Protein Immunoprecipitation Kit	Millipore	17-700
ECL chemiluminescence assay kit	Biyuntian	P0018S
TTC staining kit	Solebao	T8170
miRNA Complete Labeling and Hyb Kit	Agilent	5190-0456
Experimental models: Cell lines		
mouse cardiomyocytes HL-1	Zhong Qiao Xin Zhou Biotechnology Co., Ltd	ZQ0920
Experimental models: Organisms/strains		
BALB/c mice	SPF	N/A
Oligonucleotides		
Primers for qPCR, see Data S3	This Paper	N/A
NC inhibitor/mimic	RiboBio	N/A
miR-330-3p inhibitor/mimic	RiboBio	N/A
oe-/si-BAP1	RiboBio	N/A
oe-SLC7A11	RiboBio	N/A
si-IP3R	RiboBio	N/A
Software and algorithms		
Adobe Photoshop	Adobe	https://www.adobe.com/es/
Graphpad Prism8	GraphPad Prism Software, Inc	https://www.graphpad.com/
ImageJ	ImageJ	https://imagej.net/ij/
Cytoscape	Cytoscape	https://cytoscape.org/
R language	The R Project for Statistical Computing	https://www.r-project.org/
Other		
Agilent chip scanner	This paper	G2565CA
Agilent Feature Extraction software	This paper	N/A

EXPERIMENTAL MODEL AND STUDY PARTICIPANT DETAILS

Mouse models

60 BALB/c mice (20 ± 2 g, 4–6 weeks old) were purchased from SPF (Beijing) Biotechnology Co., Ltd. All the animals were housed in an environment with a temperature of 22 ± 1°C, a relative humidity of 50 ± 1%, and a light/dark cycle of 12/12 h. All animal studies (including the mice euthanasia procedure) were done in compliance with the regulations and guidelines of Yunnan Labreal Biotech Co., Ltd. animal care and conducted according to the AAALAC and the IACUC guidelines (IACUC Issue No. PZ20220504). Male and female mice did not affect the experiment and were therefore included in each experiment.

All experiment procedures in this study were approved and performed in accordance with the guidelines of the French Ministry of Agriculture's Animal Ethics Committee (EC Directive 2010/63/EU and French Decree 2013-118). The animal experiment of was received approval from the Experimental Animal Ethics Committee of Yunnan Labreal biotech Co., Ltd (IACUC Issue No. PZ20220504). The approved

project: Overexpressing GATA-4 mesenchymal stem cell derived exosome remodeling mitochondrial function in infarcted cardiomyocytes suppresses cardiomyocyte ferroptosis via Ap2m1/p66shc. Approval number: PZ20220504, 05/07/2020.

Cell lines culture

The mouse cardiomyocytes HL-1 (ZQ0920) was purchased from China Shanghai Zhong Qiao Xin Zhou Biotechnology Co., Ltd. Cells were cultured in MEM (Gibco, USA) supplemented with 10% fetal bovine serum (FBS, Gibco, USA) and 1% double-antibody (Gibco). Cells were incubated at 37°C in a 5%CO_2 humidified atmosphere. The cells were not cultured for longer than 2 months.

METHOD DETAILS

BMSC extraction

BMSCs were extracted by the femur and tibia of mice as previously reported[75] and co-incubated with bone marrow mesenchymal stem cell growth medium (MUXMX-90011, Cyagen Biosciences, Sunnyvale, CA, USA) containing 10% FBS. The specific procedures have been previously described in our previous publication.[26] P9 cells were selected for follow-up experiments.

Extraction and identification of exosomes

Collecting transfected BMSCs were cultured in medium with BMSC growth medium without FBS for 48 h and then centrifuged 1 h at 110,000× g and 4°C. After removing the supernatant, added the phosphate buffer saline (PBS) was resuspended through centrifugation for 1 h at 110,000×g at 4°C. Transmission electron microscopy (TEM) and nanosight analysis[43] were employed to observe and analyze the exosome morphology.

Cell transfection and treatment

Lentivirus overexpressing GATA-4[26] (Genomeditech, Shanghai, Chian) and oe-NC, as well as NC inhibitor/mimic, miR-330-3p inhibitor/mimic, oe-/si-NC, oe-/si-BAP1, oe-SLC7A11, and si-IP3R (RiboBio, Guangzhou, China) were used to transduce BMSCs and cardiomyocytes using lipofectamine 3000 reagent (Invitrogen Life Technologies, Carlsbad, CA, USA), following the manufacturer's instructions. The expression levels of genes and proteins were assessed by RT-qPCR or Western blot 24 h after transfection. Cyclosporin A (CsA, mPTP inhibition, 59865-13-3) was purchased from China, Shanghai, MedChemExpress Co., Ltd.

Bioinformatics analysis

Six exosome groups transfected with lentivirus overexpressing GATA-4 and oe-NC were randomly selected ($N = 3$). Total RNA was extracted using TRIzol reagent (Invitrogen, 15596026). The quality test for total RNA was performed using the formaldehyde-denatured gel electrophoretic assay. Next, we purified the RNA using the mirVana purification miRNA Isolation Kit (AM1561). The miRNA Complete Labeling and Hyb Kit (5190-0456, Agilent, China) was then applied to dephosphorylate and label the RNA. After hybridization, slides were washed with 0.2 SDS and 2×SSC. We scanned the slides using the Agilent chip scanner (G2565CA) and the Agilent Feature Extraction (v10.7) software to analyze the hybrid images and extract the data. Then gene expression differences and statistically significant p-values were calculated using GeneSpringGX software. Moreover, raw and normalized signal values with corresponding annotation information of all samples are shown in Table S4. Because of had 3 or more samples, the samples are clustered according to the correlation of their expression patterns (Table S5). Subsequently, the limma package of the R script[76] was used to analyze the differentially expressed genes (DEGs), and the ggplot2 and heatmap package, respectively, map volcanoes and heat maps. Screening criteria were $|\log_2 FC|>1$ and adjusted p-value <0.05.

Cell hypoxia/reoxygenation (H/R) model and co-culture

Cell hypoxia/reoxygenation (H/R) model was established as previously described.[31] HL-1 was cultured in a hypoxia cell culture incubator for 18 h in the glucose-free medium. Then, cells were placed in a 95% O_2 and 5% CO_2 incubator for 6 h. Subsequently, 1 mL of exosomes (5 μg/mL) was added in co-culture with 1×10^5 HL-1, including the Exos from BMSCs, BMSCs expressing oe-NC, and BMSCs overexpressing GATA-4.

RT-qPCR

A total RNA was extracted using a TRIzol reagent. RNA was then subjected to reverse transcription to form cDNA using the One Step Prime Script miRNA cDNA Synthesis Kit (Takara, Kyoto, Japan). For RT-qPCR procedures, we followed the instructions provided by the manufacturer of the SYBR Green PCR Master Mix (ThermoFisher, USA). The sequences of RT-qPCR primers are shown in Data S3. Finally, the $2^{-\Delta\Delta Ct}$ method was used to calculate the value, with GAPDH, U6 or β-actin as the internal reference.

Western blot

The proteins in tissue samples and cells of each group were extracted using RIPA buffer (Sigma-Aldrich, USA) containing 1% protease inhibitor and phosphatase inhibitor. Proteins were then separated using 10% SDS-PAGE gel and transferred to a polyvinylidene fluoride (PVDF) membrane (Millipore, MA, USA). The membrane was sealed with 5% skim milk at room temperature for 2 h and then incubated overnight at 4°C

with the following primary atibodies: anti-SLC7A11 (1:10000, ab175186, Abcam, UK), anti-GPX4 (1:1000, ab125066, Abcam, UK), anti-ACSL4 (1:1000, ab155282, Abcam, UK), anti-BAP1 (1:2000, ab255611, Abcam, UK), anti-Kelch-like ECH-associated protein 1 (Keap1, 1:1000, bs-3648R, bioss), anti-Nuclear factor erythroid 2-related factor 2 (Nrf2, 1:1000, bs-1074R, bioss), anti-IP3R (1:1000, ab252536, Abcam, UK), anti-MCU (1:500, HY-P80216, MedChemExpress), anti-HIF-1α (1:5000, ab179483, Abcam, UK), anti-Bcl-2 (1:2000, ab182858, Abcam, UK), and anti-Bax (1:1000, ab32503, Abcam, UK). Next, samples were washed and incubated with second antibodies conjugated with HRP (1:2000, ab205718, Abcam, UK) at room temperature for 1 h. ECL chemiluminescence solution development was used for exposure and observation. Antibody against GAPDH (1:2500, ab9485, Abcam, UK) or β-actin (1:1000, ab8226, Abcam, UK) as the control. Protein band analysis was done using ImageJ.

CCK-8 assay

The cell viability was detected using the CCK-8 test kit (Biyuntian, Beijing, China). Cells were cultured in a 96-well plate at a concentration of 3×10^3 cells per well for 1, 2 and 3 h. After each time point, 10 μL of CCK-8 solution was added to each well and incubated at 37°C. The absorbance values were measured at 450 nm using an enzyme labeling instrument (SM600, UTRAO).

Flow cytometry

The cells from each group were collected and rinsed with 200 μL of PBS solution. Early and late cell apoptosis was measured using the Annexin-V-FITC/PI apoptosis kit (7seapharmtech, Shanghai, China) following the manufacturer's instructions. Briefly, 5 μL of Annexin V-FITC and 5 μL of PI were added to each well and incubated for 15 min in a dark chamber. After that, apoptosis was detected by using FACScan flow cytometry.

The levels of lactate dehydrogenase (LDH), malondialdehyde (MDA), reduced glutathione GSH/oxidized glutathione (GSSG), superoxide dismutase (SOD) and ROS

The ELISA Kits of lactate dehydrogenase (LDH) assay kit (ml002267), malondialdehyde (MDA) assay kit (ml077384), reduced glutathione (GSH) assay kit (ml002260), oxidized glutathione (GSSG) assay kit (ml057674), and superoxide dismutase (SOD) assay kit (ml001998) were purchased from China Shanghai Enzyme-linked Biotechnology Co., Ltd. CellROX Deep Red kit (C10422) was purchased from USA Thermo Fisher Scientific Co., Ltd. Specific operation referenced the instructions of kits.

The levels assay of Fe^{2+}, Ca^{2+} and H_2S

The Ferrous Ion Content Assay Kit (BC5415, Solarbio), Fluo-8 calcium flux assay kit (ab112129, Abcam), and H_2S content Assay Kit (BC2055, Solarbio), were used to measure the concentration of Fe^{2+}, Ca^{2+} and H_2S, respectively, following the referenced the manufacturer's protocol. The microplate reader was used to detect the OD.

Analysis of the mPTP

The mPTP assay kit (C2009S) was purchased from China Shanghai Beyotime Biotechnology Co., Ltd. Briefly, cells were mixed with corresponding reagents after being centrifuged at 1000 g for 5 min. Next, cells (1×10^6) were cultured for 30 min in the dark, re-centrifuged at 1000 g for 5 min and then mixed with 400 μL buffer. After that, FACScan flow cytometry was used to evaluate the mPTP situation.

Mitochondrial membrane potential assay

The JC-1 Mitochondrial Membrane Potential Assay Kit (HY-K0601, MedChemExpress) was used to analyze the situation of mitochondrial membrane potential following a previously described approach[77] research. A fluorescence microscope was used to detect green fluorescence J-monomers and red J-aggregates. The microtome stained with uranyl acetate and lead citrate sections were reviewed for mitochondrial morphology under a TEM (JEM-2000EX, JEOL, Japan).

Immunofluorescence (IF) experiment

The cells were placed onto a 24-well plate at a density of 2×10^4 cells per well. After 24 h, the cells were washed twice with PBS, fixed with 4% paraformaldehyde, permeabilized for 10 min, and blocked with bovine serum albumin (BSA) for 1 h. The cells were then double-stained with anti-CyP-D (ab110324, Abcam, UK) or anti-Nrf2 (BF8017, Affinity) overnight at 4°C and then incubated with corresponding secondary antibodies for 1 h, followed by DAPI staining. Finally, the stained cells were observed and photographed under a fluorescence microscope (400857, Nikon, Japan).

Luciferase reporter assay

The luciferase reporter vector was cloned by BAP1-3′ untranslated region (UTR) containing the miR-330-3p binding site to generate wild type (WT) luciferase reporter plasmid, or SLC7A11 promoter was cloned by luciferase reporter pGL3 vector. After 24 h, the collected cells were lysed. The dual luciferase assay kit (Biyuntian, Beijing, China) detected the luciferase activity.

AgO2-RIP assay

The cells transfected with NC mimic, miR-330-3p mimic, after 24 h, Magna RIP RNA-Binding Protein Immunoprecipitation Kit (17-700, Millipore, Burlington, MA, USA) used to RIP analysis. The level of miR-330-3p was assessed using RT-qPCR.

Coimmunoprecipitation (CO-IP)

Cells were first lysed with IP lysis buffer and centrifuged, after which the supernatant was collected and incubated with protein A/G Sepharose (Santa Cruz Biotechnology) with the anti-BAP1 and anti-IP3R for 60 min. Then, all IPs were set overnight at 4°C. After centrifuging the beads and washing steps, the immune precipitates were assessed using Western Blot.

Pull-down assay

The pull-down assay was performed as previously described.[78,79] In short, biotin labeling with BAP1 or antisense RNA was mixed with 500 μL CO-IP buffer to dissolve. Then, 3 μg of biotinylated DNA oligoprobe or antisense probes were incubated with 50 μL streptavidin C1 magnetic beads (Invitrogen) for 1 h. SDS-PAGE was used to analyze the bound proteins in the pull-down material.

Ischemia and reperfusion (I/R) mice model

Mice were randomly divided into an ischemia and reperfusion (I/R) group and a Sham group. The animal groups were assigned random numbers using the Rand () function in Microsoft Excel. All mice were anesthetized using isoflurane inhalation (1.5%–2%). The I/R group was reperfused for 3 h after a left anterior descending coronary artery (LAD) of 45 min, following a protocol described in a previous study,[80] while the reperfusion was not performed in the Sham group. Next, both groups were treated with $Exos^{oe-NC}$, $Exos^{oe-GATA-4}$, NC inhibitor, or miR-330-3p inhibitor by tail vein injection for 3 days. Experimental mice were respectively divided into 6 different groups (n = 6 mice per group): Sham group, I/R group, I/R+$Exos^{oe-NC}$ group, I/R+$Exos^{oe-GATA-4}$ group, I/R+$Exos^{oe-GATA-4}$+NC inhibitor group and I/R+$Exos^{oe-GATA-4}$+ miR-330-3p inhibitor group.

An ultrasonic cardiogram (PHILIPS, EPIQ 7C) estimated cardiac function 3 days post-modeling. After the mice were then euthanized by cervical dislocation after anaesthetization. The 2,3,5-triphenyl tetrazolium chloride (TTC, T8170, Beijing Solebao Biotechnology Co., Ltd., Beijing, China) staining method was implemented to determine the size of a myocardial infarct.

QUANTIFICATION AND STATISTICAL ANALYSIS

The data in this paper was presented as mean +/− standard deviation (mean ± SD). GraphPad Prism 8 was used to analyze and plot the data. T-test was used to compare two groups, One-way ANOVA was used to compare multiple groups, and two-way ANOVA was used for pairwise comparison between groups. A p value < 0.05 was considered statistically significant.

ADDITIONAL RESOURCES

The datasets used and/or analyzed during the current study are available from the corresponding author on reasonable request.